Chemical Engineering Journal 383 (2020) 123196

Contents lists available at ScienceDirect

Chemical Engineering Journal

journal homepage: www.elsevier.com/locate/cej

Review

Recent progress on metal-organic frameworks based- and derived-photocatalysts for water splitting

Hanzhuo Luo[a,1], Zhuotong Zeng[b,1], Guangming Zeng[a,*], Chen Zhang[a,*], Rong Xiao[b,*], Danlian Huang[a], Cui Lai[a], Min Cheng[a], Wenjun Wang[a], Weiping Xiong[a], Yang Yang[a], Lei Qin[a], Chengyun Zhou[a], Han Wang[a], Yin Zhou[a], Suhong Tian[a]

[a] College of Environmental Science and Engineering, Hunan University and Key Laboratory of Environmental Biology and Pollution Control (Hunan University), Ministry of Education, Changsha, Hunan 410082, PR China
[b] Department of Dermatology, Second Xiangya Hospital, Central South University, Changsha 410011, PR China

HIGHLIGHTS

- The fundamentals of photocatalytic water splitting are clarified.
- Recent advances of MOFs photocatalysts for water splitting are introduced.
- Special attention has been paid to the modification or decoration strategies of MOFs.
- An insight of prospects for the MOF based- and derived- photocatalysts.

GRAPHICAL ABSTRACT

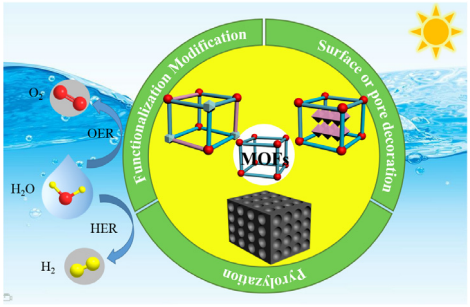

ARTICLE INFO

Keywords:
Metal-organic frameworks
Derivatives
Photocatalysts
Water splitting

ABSTRACT

Since the global energy demand and consumption increased sharply, photocatalytic water splitting becomes a promising solution to provide continuous and sustainable energy resources. However, exploring photocatalysts that could meet energy needs and put into industrial manufacture remains a challenging task. Metal-organic frameworks (MOFs), as a class of porous crystalline materials with tailorable structure and ultrahigh surface area, are regarded as an ideal candidate for photocatalysis application. Recently, their peculiar employment in photocatalytic water splitting aroused tremendous interests. Although this topic still in early stage, recent advanced experiments results have certified its potential for future application. This review starts with the fundamentals of photocatalytic water splitting, and subsequently summarizes and exemplifies recent developments of MOFs based- and derived-photocatalysts for water splitting, including water-splitting half reaction and overall water splitting. Particularly, two strategies to enhance photocatalytic performance of MOFs are specific emphasized, namely functional modification and surface or pore decoration. Finally, this review identifies the scarcities of MOFs based- and derived-photocatalysts and proposes pertinent suggestions for further improvement, whilst highlights a green future for photocatalytic water splitting.

* Corresponding authors.
E-mail addresses: zgming@hnu.edu.cn (G. Zeng), zhangchen@hnu.edu.cn (C. Zhang), xiaorong65@csu.edu.cn (R. Xiao).
[1] These authors contribute equally to this article.

https://doi.org/10.1016/j.cej.2019.123196
Received 4 June 2019; Received in revised form 6 October 2019; Accepted 15 October 2019
Available online 16 October 2019
1385-8947/ © 2019 Elsevier B.V. All rights reserved.

1. Introduction

The rapid development of industrialization has promoted the prosperity of the global economy [1], but also brought severe energy and environmental issues [2,3], such as greenhouse effect [4], water pollution [5,6] and concealable soil contamination [7,8]. It is unambiguous that continuing utilize of traditional fossil fuels will exacerbate these problems. Recently the global energy consumption and climate changes have stimulated researchers to exploit renewable and sustainable energy sources [9]. Solar energy which represents an enormous and sustainable resource stem from natural has the largest potential to provide powers for energy conversion reaction. In this regard, photocatalytic water splitting into hydrogen and oxygen sources has been recognized applicable and eco-friendly technology [10]. Hydrogen has been expected to replace traditional fossil fuels due to its clean, non-toxic byproducts and storable characteristics. Accordingly, how to enhance hydrogen evolution reaction (HER) rate has become a hot topic in this field. The research on more sluggish and challenging half reaction, i.e. oxygen evolution reaction (OER), has also developed rapidly because its great influence on overall water splitting rate.

Although pioneer research on solar energy to chemical energy conversion was reported in 1972 by Honda and Fujishima [11], there are still few photocatalysts that can meet actual energy demand at present. In fact, it is unrealistic to rely on materials with only unitary property to pursue optimal photocatalytic performance [12]. For example, inorganic semiconductors TiO_2, which generally possess excellent stability during photocatalytic reaction [13], own wide band gap (3.2 eV) [14] and poor quantum yield [15]. On the contrary, the photoactivity of organic photocatalysts could be well tuned by introducing functional groups [16], but their stability in solution remains a severe problem [17]. Despite researchers have applied various methods to improve energy conversion efficiency of traditional photocatalyst [18], more efforts should be put into the development of alternative photocatalyst.

Metal-organic frameworks (MOFs), constructed by metal nodes (metal clusters or ions) and organic linkers, have attracted widespread attention owing to its structural diversity and tailorability, ultrahigh surface area and crystalline nature [19]. It has been applied in many applications, such as CO_2 reduction [20], water splitting [21], organic pollutants degradation [22], adsorption [23,24], catalysis [25] and sensing [26]. It is noteworthy that there has been a growing interest in the use of metal-organic frameworks as photocatalysts for overall water spitting and water-splitting half reaction. According to the data from Web of Science in Clarivate analytics (Fig. 1), more and more papers on metal-organic frameworks have emerged in a few years from the start of the studies to an explosive growth. The number of publications further

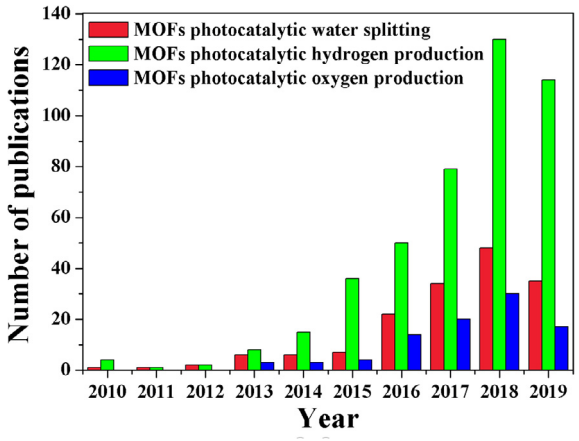

Fig. 1. The current research trends of metal-organic frameworks in photocatalytic water splitting (the data from Web of Science).

indicating the high importance and tremendous research interests in this area.

Compared with traditional photocatalysts, MOFs have several outstanding advantages in photo-induced reaction. For instance, the desirable topology and multiple porous structure of MOFs can promote the substrate molecules transfer and diffusion [27], which inherited the advantages of porous materials such as zeolite [28], carbon nanomaterials [29,30], covalent organic frameworks (COFs) [31] and DNA hydrogels [32]. Additionally, abundant active sites for catalytic reaction are exposed which succeed to the porous property and high surface area of MOFs [19]. Most outstanding merit is the physical and chemical properties of MOFs which could be enhanced by sensible designing and tuning the composition and structure, thus considerable reports have devoted to pursue the optimal modification strategy of MOFs photocatalysts for specific photo-induced application [33]. In recent years, several reviews related to MOFs in photocatalytic water splitting have been published. For instance, Wang and co-workers summarized the application of MOFs based composites in photocatalytic and electrocatalytic water splitting [34]. Recently, Shi et al. discussed the photocatalytic application of MOFs based composites and MOFs derivatives for hydrogen production from water [35]. These works reflected the rapid development of MOFs in photocatalytic water splitting. However, the bottlenecks of overall water splitting and water-splitting half reaction for practical application are still unrevealed. Additionally, the functionalization and decoration strategies of MOFs for further improvement in photocatalytic water splitting application are urgently required to be clarified.

Herein, recent progress of MOFs based photocatalysts and MOFs derivatives for water splitting, i.e. oxygen evolution reaction (OER) and hydrogen evolution reaction (HER), is exemplified and summarized. These advances of MOFs based photocatalysts are clarified into two types according to the mode of modification, i.e. functional modification and surface or pore decoration. As a supplementary, the developments of MOFs derivatives which obtained by pyrolyzation are also concluded. Finally, the critical challenges and barriers of this field are presented and the potential solutions are proposed.

2. Fundamentals of photocatalytic water splitting

Photocatalytic water splitting mechanism includes following steps (Fig. 2) [36]: First, after activated by light irradiation, the electrons of photocatalyst transfer from valence band (VB) to conduction band (CB) while the holes of photocatalyst are left in the VB, thus creating electron-hole pairs. The photogenerated electrons and holes subsequently migrate to the surface of the photocatalyst while some of them recombined in this process. Finally, electrons and holes on the surface of photocatalyst react with water molecules to generate hydrogen and oxygen, respectively. Corresponding to the three steps some requirements are highlighted to enhance catalytic performance of photocatalysts. In terms of light harvesting efficiency, there are three compositions in sunlight and can be divided by wavelength: infrared rays ($\lambda > 800$ nm), visible light (400 nm $< \lambda <$ 800 nm) and ultraviolet rays ($\lambda < 400$ nm). However, ultraviolet ray accounts for a small fraction (about 4%) of the entire solar energy while visible light (about 53%) and infrared light (about 43%) holds great proportion [37]. Owing to larger proportion that visible light occupied, harvesting visible light is essential for improving energy conversion efficiency. Particularly, some advanced semiconductors even accept near-infrared (NIR) light for water splitting [38,39]. Secondly, the photocatalytic performance is mainly depended on the separation efficiency of electrons and holes. Strategies such as constructing heterojunction to prolong charges lifetime, shrinking particle size to reduce the distance that electrons reach to the surface, adding sacrificial agents to consume electrons or holes provide avenues for suppress recombination [40]. Lastly, high surface area and massive active sites can increase the contact area between photocatalyst and substrate, i.e. water molecules,

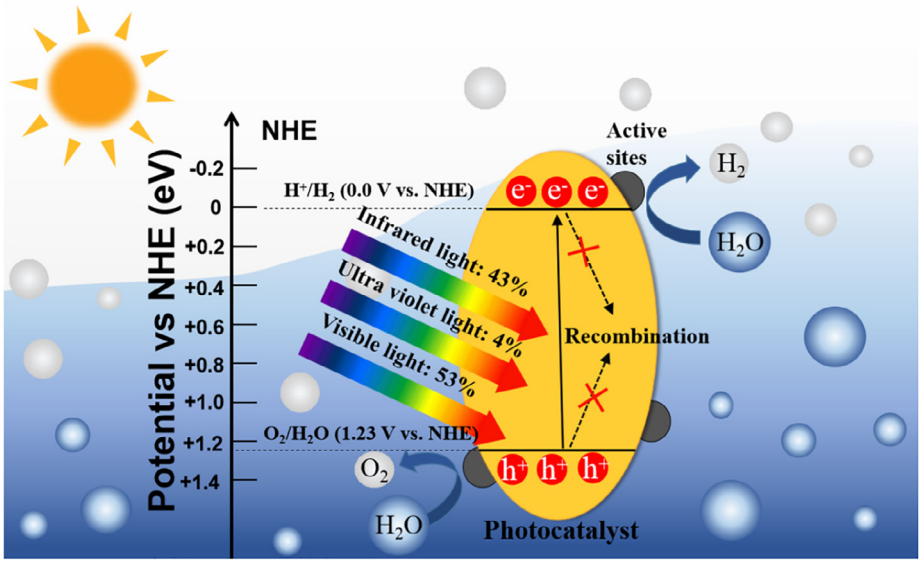

Fig. 2. Main processes in photocatalytic water splitting and corresponding strategies to enhance photocatalytic performance.

thus improving the rate of water splitting reaction.

In thermodynamically, overall water splitting (Eqs. (1)) is an uphill reaction ($\triangle G^{\circ}$ = 237 kJ/mol correspond to 1.23 eV), and it is composed of two half reactions, i.e. OER (Eq. (2)) and HER (Eq. (4)). Unlike water reduction reaction, water oxidation is a sluggish reaction [13]. Hence, a large number of holes accumulate on the surface of photocatalyst during overall water splitting process. However, promoting excessive oxygen evolution may result in competition with hydrogen for electrons and subsequently generate superoxide radicals [37]. Consequently, it is essential to properly control the rate of oxygen evolution in overall water splitting. Besides, the CB and VB edges of photocatalysts must be suitable to trigger overall water splitting. In other words, the CB edge of photocatalysts should be relatively negative than the redox potential of H^+/H_2 (0.0 V vs. NHE), while the VB edge should be relatively positive than the redox potential of O_2/H_2O (1.23 V vs. NHE) [41].

Overall water splitting

$$H_2\,O \rightarrow H_2 + 1/2O_2 \quad (1)$$

Water oxidation half reaction (oxygen evolution dominate)

$$4h^+ + 2H_2\,O \rightarrow O_2 + 4H^+ \quad (2)$$

$$A + e^- \rightarrow A^-(\text{A is an electron acceptor}) \quad (3)$$

Proton reduction half reaction (hydrogen evolution dominate)

$$2H^+ + 2e^- \rightarrow H_2 \quad (4)$$

$$D + h^+ \rightarrow D^+(\text{D is an electron donor}) \quad (5)$$

To meet specific industrial needs, water-splitting half reaction gained the popularity in recent years due to its less difficulty in gas separation. In some cases, sacrificial electron donors or electron acceptors are added to consume holes or electrons and accelerate water-splitting half reaction (Eqs. (3) and (5)) [42]. In recent years, several reports also suggested combine value-added chemicals oxidation reaction with H_2-producing half reaction [43], which increasing overall reaction rate and saving costs. Compare with overall water splitting, the lower restrictive band gap requirement of water-splitting half reaction also broaden the choice of photocatalysts.

With regard to photocatalysts, two properties are essential to induce photocatalytic water splitting reaction, i.e. catalytic property and photosensitivity [44]. MOFs have unique advantages in these two properties. When it comes to catalytic property of MOFs, some MOFs have been considered as microporous semiconductor as it undergoes electrons and holes separation under light irradiation [45]. Nevertheless, most MOFs are gradually accepted as poor electrical conductivity [46], which is ascribe to the symmetry mismatch of ligand and orbital as well as their energy-level alignment inadequacy [47]. It is the porosity of MOFs that compensate this drawback, which can be explained to the short distance between redox sites and the evolution position of photogenerated carriers. Moreover, these pores also allow efficient diffusion of the reactants and intimate contact with active sites. As for photosensitivity, some MOFs, such as MIL-101, MIL-100, MIL-53 (MIL, Materials of Institut Lavoisier), possess excellent photoactivity and even respond in the visible light range. Moreover, due to its high designability, components functionalization can be utilized as efficient strategy to strengthen MOFs visible light and even NIR light response, which reflected the superiority of MOFs over traditional semiconductor such as ZnO, CdS and TiO_2 [48]. For example, the introduction of amino group into the organic ligands of Ti-MOF can shift the band as they devote 2p electrons to aromatic linker [49]. Besides, the pore size of MOFs is positively correlated with the length of organic ligands, which is beneficial to decorate functional substances of different sizes as needed.

MOFs have been proved to be applied in photocatalytic water splitting. Several pristine MOFs show good photocatalytic activity for water splitting without doing further post-modification. For example, Shi et al. [50] synthesized Cu-I-bpy (bpy = 4,4′-bipyridine) without additional photosensitizers and cocatalysts, which showed good photocatalytic hydrogen production rate (7.09 $mmol{\cdot}h^{-1}{\cdot}g^{-1}$). In addition, the method for combining with photosensitizing units and MOFs is also beneficial for highly photocatalytic activity for hydrogen production, such as some well-known molecular dyes ($Ru(bpy)_3Cl_2$ and less expensive porphyrines, etc.) as photosensitizing linkers [51]. However, some pristine MOFs are still restricted by limited visible light response and short life time of excited carriers, etc. On the other hand, development of novel MOFs with above mentioned merits remains a challenge task. Based on the existing pristine MOFs, it is sensible to employ effective modification or decoration strategies to make it possess better photocatalytic property. In this regard, two typical strategies are emphasized in this review: functional modification refers to the integration of foreign groups or ions into metal center or organic ligand of MOFs, while surface or pore decoration refers to the decoration of foreign functional substances on surface or pores of MOFs.

Table 1
Photocatalytic water splitting performance of MOFs by functional modification.

Functional modification	MOFs	Metal clusters/core	Ligands	Sacrificial reagent	Target reaction	Production rate ($mmol{\cdot}h^{-1}{\cdot}g^{-1}$)	Recycled times	Ref.
Functional groups modification	Pt/NH_2-MIL-101(Cr)	Cr-O cluster	ATA	TEOA	HER	0.6 $mmol{\cdot}h^{-1}{\cdot}g^{-1}$	5	[56]
	HNTM-Ir/Pt	Zr-O cluster	porphyrin	TEOA	HER	0.2 $mmol{\cdot}h^{-1}{\cdot}g^{-1}$		[52]
	Co@MOF	Ti-O cluster	ATA, L^{H2}	TEA	HER	22.5 $mmol{\cdot}h^{-1}{\cdot}g^{-1}$	3	[74]
	MIL-101(Fe)–NH_2	Fe-O cluster	BDC-NH_2	$Na_2S_2O_8$	OER	61.8 $mmol{\cdot}h^{-1}{\cdot}g^{-1}$		[58]
	PMOF	Ti-O cluster	porphyrin	ascorbic acid	HER	8.52 $mmol{\cdot}h^{-1}{\cdot}g^{-1}$	3	[59]
	Pt/Cd-MOFs	Cd-O cluster	H_2DSPTP	TEOA	HER	1.2 $mmol{\cdot}h^{-1}{\cdot}g^{-1}$	5	[63]
	Pt/Cu-MOFs	Cu–O cluster				7.3 $mmol{\cdot}h^{-1}{\cdot}g^{-1}$	8	
	$RhOH_2$@UiO	Zr-O cluster	BPDC	TEOA	HER	10.4 $mmol{\cdot}h^{-1}{\cdot}g^{-1}$		[69]
	Pt(1.5)/Ti-MOF-NH_2	Ti-O cluster	ATA	TEOA	HER	≈ 0.4 $mmol{\cdot}h^{-1}{\cdot}g^{-1}$	3	[73]
	Ti-MOF-Ru(tpy)$_2$	Ti-O cluster	Ru(tpy)$_2$	TEOA	HER	≈ 0.4 $mmol{\cdot}h^{-1}{\cdot}g^{-1}$	3	[53]
Metal doping modification	NH_2-UiO-66(Zr/Ti)	Zr-O cluster, Ti-O cluster	ATA	TEOA	HER	7.8 $mmol{\cdot}h^{-1}{\cdot}g^{-1}$		[76]
	$Zn_{0.986(12)}$TCPP-[AlOH]$_2$	Al-O cluster, Fe-O cluster	$Zn_{0.986(12)}$TCPP	–	–	–		[78]

3. MOFs based composites as photocatalysts

3.1. Functionalization modification of MOFs

Characteristic properties of MOFs mostly depend on their composition, which will further influence their photocatalytic performance. Hence, it is extraordinary important to modify organic linkers and metal centers of MOFs for expected chemical and physical properties, which leads to two ways of functionalization: functional groups modification and metal doping. The photocatalytic water splitting performance of MOFs by functional modification are concluded in Table 1.

3.1.1. Functional groups modification

Decoration of the organic linkers of MOFs can decrease the band gap energy to some extent. According to the formula: λg (nm) = 1240/Eg (eV), the light absorption edge could expand to the visible light or even NIR light region. For instance, functional groups such as amino and porphyrins [52] can be insert into organic linkers to decrease the band gap energy and expand the light absorption edge of MOFs. Not only decrease the band gap energy, some reports manifested that metal complex can even expand the choice of sacrificial agents of water splitting system [53].

Amino groups have been inserted into organic linker to expand the light absorption edge of MOFs. For example, UiO family is preferred by researchers of solar energy conversion [54]. Owing the highly water-stable property [51], UiO have an attractive prospect for photocatalytic water splitting. Sliva et al. compared the photocatalytic performance of UiO-66 and ATA modified UiO-66-NH_2 for HER [55], and the results suggested that introducing amino to BDC ligand led to red shift of the adsorption from 300 to 440 nm without changing the structure of MOFs. Similarly, the photocatalytic hydrogen production of amino functionalized MIL-101(Cr) has been explored by Wen and co-workers [56], and obvious hydrogen generation of pure NH_2-MIL-101 was observed in the presence of rhodamine B (RhB) photosensitizer. From the UV–visible spectra of supernatant solutions, the intensity and position of the absorption peak of RhB did not change, which means that Pt/NH_2-MIL-101 possesses high chemical stability. Since the photocatalytic activities of various Fe-based MOFs (MIL-101(Fe), MIL-126(Fe), MIL-100(Fe), MIL-88(Fe) and MIL-53(Fe)) for water oxidation have been investigated in visible light [57], Chi and co-workers also have explored the photocatalytic water oxidation capacity of different iron-based MOFs (i.e. MIL-53(Fe), MIL-88(Fe) and MIL-101(Fe)) as well as their amino functionalized counterparts under visible light [58].

Except amino group, porphyrins are also used to enhance the photosensitivity of MOFs. Recently, a PMOF which consist of Ti-oxo clusters and porphyrin has been synthesized [59], and the light adsorption range have been enlarged to 700 nm. Benefiting from this, it exhibits excellent photocatalytic hydrogen production rate (8.52 $mmol{\cdot}h^{-1}{\cdot}g^{-1}$). In addition to being introduced into MOFs as an organic ligand, porphyrin molecules can also improve the performance of photocatalysts by metallization. For example, He et al. not only synthesized zirconium–porphyrinic hollow nanotubes MOF (denoted as HNTM) but immobilized single noble-metal atom (Pd, Ru, Pt, Au, Ir) on porphyrinic linker by solvothermal method [52]. It has been discovered that HNTM-Ir/Pt owned the best performance for photocatalytic hydrogen generation (201.9 $\mu mol\,h^{-1}\,g^{-1}$), in which porphyrinic-Pt units served as catalysts and porphyrinic-Ir units acted as photosensitizers.

Other photosensitizers also have been introduced into MOFs as organic linkers. For example, Hou and co-workers encapsulated a Ru-based molecular photosensitizer and a Pt-based molecular catalyst into UiO-67 by mix-and-match approach [60]. In this case, the excited Ru-based molecular photosensitizer transfers electrons to Pt-based catalyst after light irradiation, then water was reduced to hydrogen in Pt-catalytic center of MOFs. Finally, the excited state of Ru-based molecular photosensitizer back to the ground state by sacrificial electron donor, i.e. EDTA-2Na. Kim et al. have embedded a Pt(II) molecular catalyst and an Ir(III)-based photosensitizer into bipyridine-embedded UiO-67 MOF (BUiO) [61], and the as-synthesized MOF was termed as self-healing system that spontaneously repair the catalyst and photosensitizer during HER by controlling the ratio of 2,2′-bipyridine-5,5′-dicarboxylate to Pt. Cd-based MOFs also have been functionalized by photosensitizer for photocatalytic water splitting. For instance, the photoactivity of Cd-based MOFs have been enhanced by embedding eco-friendly dye, i.e. Eosin Y (EY), into linker [62], and the as-synthesized Cd-EY1 photosensitizer cooperated with co-catalyst [Co(bpy)$_3$]Cl$_2$ (bpy = 2,2′-bipyridine) to facilitate electron transmission and improve hydrogen production rate. Additionally, in the case of the same organic linker, Cd-based MOF has been compared with Cu-based MOF [63]. The spectra response range of Cu-based MOF was wider than Cd-based MOF, and it also could induce hydrogen evolution under NIR light irradiation. Furthermore, without any cocatalyst and photosensitizer, two novel Cu-based MOFs have been reported to catalyze photocatalytic hydrogen production half reaction under visible light or even NIR light irradiation [64].

In recent works, the metal complex catalysts are introduced into MOFs which serve as superior supports [65]. Pullen and co-workers prepared UiO-66-[FeFe](dcbdt)(CO)$_6$ (dcbdt = 1,4-dicarboxylbenzene-2,3-dithiolate) MOF by PSE strategy [66], in which UiO-66 MOF provided a platform to improve [FeFe](dcbdt)(CO)$_6$ moiety structural stability. The as-synthesized MOF exhibited excellent hydrogen production rate in water at pH = 5. Likely, molecular catalysts [Fe$_2$(cbdt)(CO)$_6$] ([FeFe], cbdt = 3-carboxybenzene-1,2-dithiolate) have been covalently incorporated into amino-functionalized MIL-101(Cr) (denoted as MIL-101-NH-[FeFe]) [67], and the MIL-101-NH-[FeFe] with

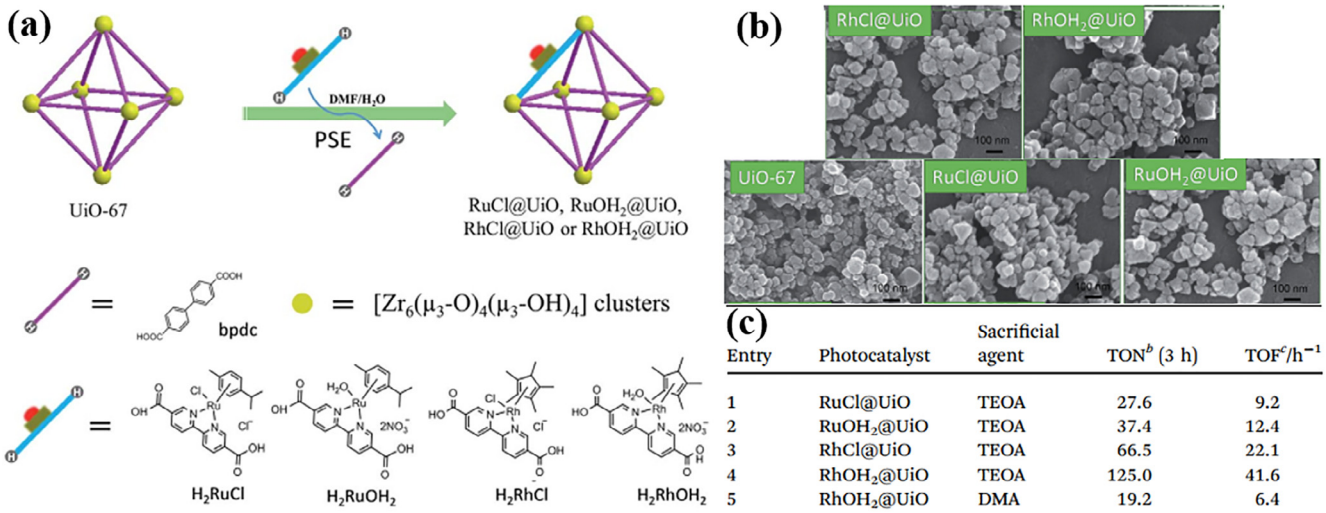

(c)

Entry	Photocatalyst	Sacrificial agent	TON[b] (3 h)	TOF[c]/h^{-1}
1	RuCl@UiO	TEOA	27.6	9.2
2	$RuOH_2$@UiO	TEOA	37.4	12.4
3	RhCl@UiO	TEOA	66.5	22.1
4	$RhOH_2$@UiO	TEOA	125.0	41.6
5	$RhOH_2$@UiO	DMA	19.2	6.4

Fig. 3. (a) Installation of heterogeneous MOFs catalysts through PSE method. (b) SEM of the as-synthesized UiO-67, and RuCl@UiO, $RuOH_2$@UiO, RhCl@UiO, $RhOH_2$@UiO MOFs. (c) Results for RuCl@UiO, $RuOH_2$@UiO, RhCl@UiO and $RhOH_2$@UiO under optimized condition for short-term (3 h) photocatalytic hydrogen evolution. Reprinted with the permission from Ref. [69]. Copyright 2018 Royal Society of Chemistry.

different catalysts concentration all displayed better catalytic capacity for hydrogen production than pure MIL-101-NH_2. Similar research also has been reported by Sasan et al., they incorporated photosensitizer porphyrin and active catalyst sites biomimetic [Fe_2S_2] into Zr based MOF [68]. Recently, four Rh- and Ru-based molecular complexes was created and encapsulated into UiO-67 by exchange with the original dicarboxylate bpdc ligands [69], namely RuCl@UiO, $RuOH_2$@UiO, $RhOH_2$@UiO and RhCl@UiO (Fig. 3a). The optical band gap of UiO-67 (~3.5 eV) rapidly reduced to around 2.4 eV after PSE process while there was no significant change in structure and particles size (Fig. 3b), and RuCl@UiO, $RuOH_2$@UiO, RhCl@UiO, $RhOH_2$@UiO MOFs were all responsive to visible light (400–500 nm). Moreover, photocatalytic experiment of hydrogen production indicated that $RhOH_2$@UiO perform best, which the turnover number (TON) was 125.0 and the turnover frequency (TOF) was 41.6 h^{-1} (Fig. 3c). A well crystalline MIL-125(Ti) was first reported in 2009 [70], which is consist of titanium-oxo-hydroxo clusters and terephthalate acid (H_2BDC) linkers. However, the optical band gap energy of MIL-125(Ti) is 3.6 eV [71], which indicates its poor photoactivity in visible light range. Horiuchi et al. synthesized an amino-functionalized Ti(IV) based MOF (denoted as NH_2-MIL-125) which has visible light adsorption ($\lambda > 500$ nm) and then Pt nanoparticles (NPs) were loaded by photodeposition method [72]. As a result, the photocatalytic activity of Pt/NH_2-MIL-125 for hydrogen production was improved. Moreover, this group proposed that the optimized amount of Pt NPs deposition was 1.5 wt% [73]. The Pt(1.5)/Ti-MOF-NH_2 had no significant loss of photocatalytic activities after three cycles of experiments. In addition, from XRD and FT-IR measurements, the diffraction peaks corresponding to the MIL-125 structure were unchanged. This means the organic linker with amino group stably exist during the reaction. Owing to the fact that this system was limited by available longest light wavelength and irreplaceable sacrificial electron donor (i.e. TEOA, triethanolamine), Ru complex was employed as organic linker by solvothermal method with Ru(tpy)2, methanol, DMF and tetrapropyl orthotitanate (TPOT) as raw materials [53]. In this case, Ti-MOF-Ru(tpy)$_2$ not only achieve excellent stability and steady hydrogen production after three cycles, but its structure remains the unchanged, which can be confirmed by XRD. Ultimately the visible light adsorption wavelength for hydrogen production was up to 620 nm and the choice of sacrificial agent was also expanded. Moreover, molecule cobalt (Co) catalyst also have been encapsulated into a photoactive NH_2-MIL-125(Ti) (denoted as Co@MOF) by 'ship-in-the-bottle' approach (Fig. 4a) [74], and the Co complex was connected to the Ti oxo-cluster of MOF, which was beneficial for well dispersed of Co molecules in MOF cavities (Fig. 4b–e). Since the lower catalytic potential of Co@NH_2-MIL-125(Ti) than the lowest unoccupied molecular orbital (LUMO) of NH_2-MIL-125(Ti), the photogenerated electrons of organic linkers rapidly transfer to Co species while the holes consumed by sacrificial electron donor. Consequently, the Co@MOF showed excellent photocatalytic activity with higher to 20-fold hydrogen production rate than pristine Co-free MOF. Moreover, after recycling tests, the activity of Co@MOF remained unchanged and its internal cobalt did not leach, indicating that the composite is stable in water. Through the several cycles of experiments, the Co@MOF retained the catalytic activity very well and the active substance was not detected in the solution. This means that the Co@MOF is very stable in solution. It can be inferred that its crystallinity has unchanged in the solution. Furthermore, Iglesias-Juez et al. illuminated the structure and property of photocatalytic Co@NH_2-MIL-125(Ti) for hydrogen production by Electron Paramagnetic Resonance (EPR) and X-ray absorption spectroscopy (XAS) analysis [75].

3.1.2. Metal doping

Metal doping is regarded as an efficient method to improve photocatalytic performance of MOFs. The affluent coordination sites in MOFs afford spaces for stabilizing foreign metals. The doped metals serve as mediators to facilitate electron transfer, greatly boosting the photocatalytic activity. Inspired by the application of metal doping in semiconductor, Sun et al. employed a post-synthesis exchange (PSE) method to prepare a Ti-replaced NH_2-UiO-66(Zr/Ti) [76]. Density functional theory (DFT) and electron spin resonance (ESR) were employed to unveil the path of electron transmission: The excited 2-aminoterephthalic acid (ATA) ligand transfer electrons to Ti^{4+} (larger probably to Ti^{4+} rather than Zr^{4+}) and the reduced Ti^{3+} acts as electron mediator that donate electrons to Zr^{4+}, and the efficient charge transfer result in higher photocatalytic activity of NH_2-UiO-66(Zr/Ti) as the amount of hydrogen production was equivalent to 1.5 times of pristine NH_2-UiO-66(Zr). Besides, since the previous work that water-stable $Zn_{0.986(12)}$TCPP-[AlOH]$_2$ composed of Al^{3+} ions as metal center and porphyrin metallized by zinc as a linker has been reported [77], Aziz et al. overcame the shortcomings of $Zn_{0.986(12)}$TCPP-[AlOH]$_2$ that slightly wide band gap and low efficiency of spatial charge separation by partial substitution Al by Fe at metal centers [78]. Therefore, the band gap (1.9 eV) has been well tuned and effective suppressed the electron-hole recombination.

Except functional groups modification and metal doping, other factors also have impact on the photocatalytic performance of MOFs.

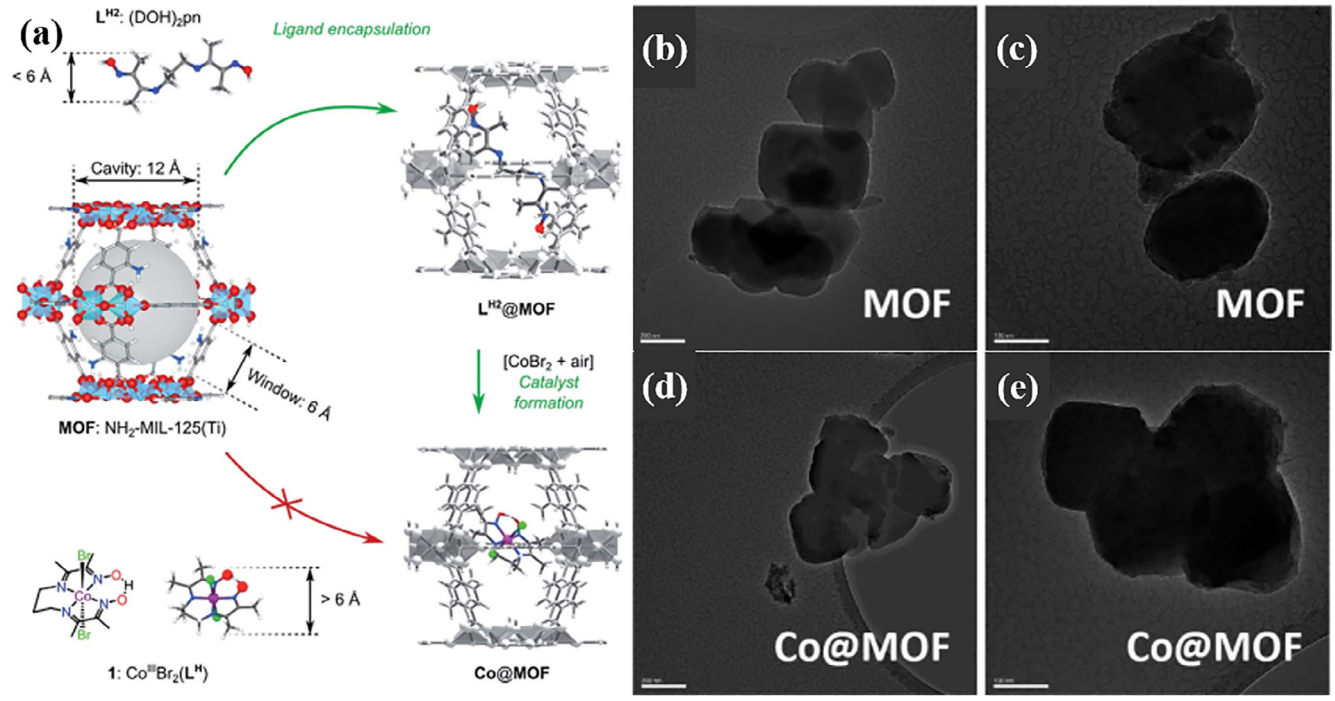

Fig. 4. (a) 'Ship-in-the-bottle' synthetic strategy followed for assembling of Co@MOF. (b)–(e) TEM of pristine NH_2-MIL-125(Ti) (200 nm-b; 100 nm-c) and Co@MOF (200 nm-d;100 nm-e). Reprinted with the permission from Ref. [74]. Copyright 2015 Royal Society of Chemistry.

For instance, owing chemical/thermal stability and easy-controlled synthesis advantages, ZIF-8(Zn) become one of the most typical MOFs materials. Nevertheless, the photocatalytic application of ZIF-8(Zn) has restricted by its large band gap energy (5.1 eV) and poor visible light response. The band edge position of ZIF-8(Zn) has been adjusted by linker mix-and-match approach [79], which indicated that the band position could be well tuned by mixing linkers of low-lying conduction edge with high-lying valence edge.

In summary, benefiting from its design flexibility, the metal clusters and the organic ligands of MOF can be easily functionalized, such as partial substitution of metal center and introduction of functional groups into organic ligands. Besides, the stability of MOFs in photocatalytic process should take into consideration, especially in water splitting system which the pH of the aqueous solution fluctuate. According to previous research [80,81], some familiar MOFs based photocatalysts could retain crystallinity and activity in water, weak acid and base, such as UiO-66, MIL-100, MIL-53, ZIF-8 and etc. Some efforts also have been devoted to strengthen the stability of novel MOFs. For example, a novel MOF consisted of 9-phenylcarbazole-3,6-dicarboxylic acid (H_2PDA) and $Zn(NO_3)_2{\cdot}6H_2O$ have been synthesized [82]. Because pure Zn-PDA_2 was easily decomposed, thus the hydrogen production of pure Zn-PDA_2 is reduced by half after one cycle. From ICP-MS analysis of the supernatant solution, about half of the Zn leaks into the solution. However, for PDMS-coated Zn-PDA_2, only 3% of Zn leached in solution after 5 cycles (PDMS = polydimethylsiloxane). From the PXRD images of the PDMS@Zn-PDA_2 soaked in water or alkaline solution (PH = 10) for five days, they found the sample still remains intact.

3.2. Surface or pore decoration of MOFs

Even though functional modification is beneficial to improve the photocatalysis property of MOFs to some extent, further enhance photocatalytic performance should rely on more efficient strategy, i.e. surface or pore decoration [83]. The superiority of surface or pore decoration compared with functional modification is reflected in the following aspects: Firstly, the band gap of MOFs could be well tuned when combine with other typical photoactive substances, therefore enlarge the visible light and even NIR light adsorption scope of these composites. In some cases, dual-excitation of typical photoactive substances and MOFs is beneficial to boost quantum yield. Secondly, surface or pore decoration could efficient separate electrons and holes pairs spatially. Besides, the intimate contact between MOFs and photoactive substances could induce the recombination of lower-position CB electrons and higher-position VB holes, promoting the separation of higher-position CB electrons and lower-position VB holes. Additionally, surface or pore decoration can equip MOFs with more active sites for catalytic reaction. The photocatalytic performance of MOFs based photocatalysts for water splitting are concluded in Table 2.

3.2.1. Corporation with semiconductor

Except judicious construct metal center and organic linker of MOFs, there is a facile solution of assemble MOF with semiconductor to narrow the band gap of MOF. There are two merits of this heterogeneous photocatalysts: one is to enlarge light adsorption edge to visible or even NIR light region and another is to realize efficient separation of electron and holes.

Graphitic carbon nitride (g-C_3N_4) has received great concerns in recent years [84], and its various nanostrcure morphologies have been developed to improve chemical and optical property of bulk g-C_3N_4 [85,86]. As a typical metal-free polymeric semiconductor [87], g-C_3N_4 is mainly composed of C, H and N, and it has been applied in photocatalytic reaction due to its high chemical and thermal stability [88], low economic cost and excellent visible-light capacity [89]. To improve the photocatalytic activities of UiO-66 with wide band gap (3.5 eV), Wang et al. synthesized several hybrids that were consist of g-C_3N_4 and UiO-66 MOF with different ratios by annealing the mixture of them at Ar atmosphere [90] (Fig. 5a). Along with mass fraction of g-C_3N_4 in hybrids increases the surface of this hybrid became rough and uneven till fully coated (Fig. 5b–d). Owing to the flexible layered structure and narrow band gap (2.7 eV) of g-C_3N_4 that could wrap or anchor on UiO-66 MOF and transfer electrons to UiO-66 MOF, the photocatalytic hydrogen production amount of these hybrids increased as the mass fraction of g-C_3N_4 (below 50%) in hybrid increase (Fig. 5e). However,

Table 2
Photocatalytic performance of MOFs decorated by different substances.

Strategies	MOF photocatalysts	details	Target reaction	Sacrificial reagent	Production rate ($mmol \cdot h^{-1} \cdot g^{-1}$)	Recycled times	Ref.
Corporation with semiconductor	UiO-66	g-C_3N_4	HER	ascorbic acid	≈1 $mmol \cdot h^{-1} \cdot g^{-1}$		[90]
	NH_2-MIL-125(Ti)	g-C_3N_4, $Ni_{15.8}Pd_{2.1}$ NPs	HER	TEOA	8.7 $mmol \cdot h^{-1} \cdot g^{-1}$	3	[94]
	NH_2-MIL-125(Ti)	g-C_3N_4	HER	TEOA	≈0.027 $mmol \cdot h^{-1} \cdot g^{-1}$		
	UNiMOF (2D)	g-C_3N_4 nanosheets	HER	TEOA	0.4006 $mmol \cdot h^{-1} \cdot g^{-1}$	3	[91]
	MIL-101(Cr)	CdS	HER	lactic acid	≈7.5 $mmol \cdot h^{-1} \cdot g^{-1}$	4	[96]
	MIL-101(Cr)	Au, CdS	HER	Na_2S and $NaSO_3$	25 $mmol \cdot h^{-1} \cdot g^{-1}$	4	[98]
	MIL-101(Cr)	CDs, CdS	HER	lactic acid	0.488 $mmol \cdot h^{-1} \cdot g^{-1}$	4	[99]
	UiO-66	$Cd_{0.5}Zn_{0.5}S$, g-C_3N_4	HER	Na_2S and $NaSO_3$	1.2811 $mmol \cdot h^{-1} \cdot g^{-1}$	3	[101]
	UiO-66	CdS, M_OS_2	HER	lactic acid	32.5 $mmol \cdot h^{-1} \cdot g^{-1}$	4	[103]
	NH_2-MIL-125(Ti)	Cu_2O	HER	TEOA	11.0555 $mmol \cdot h^{-1} \cdot g^{-1}$	5	[104]
	UiO-66-NH_2	MoS_2 quantum dots	HER	TEOA	0.8344 $mmol \cdot h^{-1} \cdot g^{-1}$		[113]
	ZIF-8	TiO_2 HNPs	HER	methanol	0.2542 $mmol \cdot h^{-1} \cdot g^{-1}$	5	[105]
	UiO-66	CdS NPs	HER	ascorbic acid	4.7 $mmol \cdot h^{-1} \cdot g^{-1}$		[97]
	MIL-101(Cr)	CdS NPs	HER	Na_2S and $NaSO_3$	1.9 $mmol \cdot h^{-1} \cdot g^{-1}$		[143]
	MIL-101(Cr)	CdS NPs, 1,1′-bi-2-naphthol functionalized PTC	HER	Na_2S and $NaSO_3$	94.9 $mmol \cdot h^{-1} \cdot g_{CdS}^{-1}$		
	MIL-101(Cr)	CdS NPs, nitrate functionalized PTC	HER	Na_2S and $NaSO_3$	36.6 $mmol \cdot h^{-1} \cdot g_{CdS}^{-1}$		
	MIL-101(Cr)	CdS NPs, bromoacetic functionalized PTC	HER	Na_2S and $NaSO_3$	39.1 $mmol \cdot h^{-1} \cdot g_{CdS}^{-1}$		
	MIL-101(Cr)	CdS NPs, benzoic functionalized PTC	HER	Na_2S and $NaSO_3$	53.3 $mmol \cdot h^{-1} \cdot g_{CdS}^{-1}$		
	MIL-101(Cr)	CdS NPs, isonicotinic functionalized PTC	HER	Na_2S and $NaSO_3$	61.8 $mmol \cdot h^{-1} \cdot g_{CdS}^{-1}$		
	UiO-66-NH_2	$Cd_{0.2}Zn_{0.8}S$ NPs	HER	Na_2S and $NaSO_3$	5.8465 $mmol \cdot h^{-1} \cdot g^{-1}$	4	[100]
Decoration of graphene	UiO-66-NH_2	Graphene(50 wt%)	HER	TEOA	41.4 $mmol \cdot h^{-1} \cdot g^{-1}$	4	[109]
	UiO-66	graphene, Ni_4S_3(20 wt%)	HER	TEOA	≈2.8 $mmol \cdot h^{-1} \cdot g^{-1}$		[110]
	UiO-66	graphene	HER	TEOA	≈0.015 $mmol \cdot h^{-1} \cdot g^{-1}$		
	Cu-BTC	electrostatic interaction assembly of ZnO/GO and Cu-BTC	HER	methanol	0.191 $mmol \cdot h^{-1} \cdot g^{-1}$		[111]
	Cu-BTC	ZnO/(Cu-BTC)/GO complex	HER	methanol	≈0.064 $mmol \cdot h^{-1} \cdot g^{-1}$		
	UiO-66	CdS, RGO	HER	Na_2S and $NaSO_3$	13.8 $mmol \cdot h^{-1} \cdot g^{-1}$		[112]
	UiO-66	CdS	HER	Na_2S and $NaSO_3$	11.2 $mmol \cdot h^{-1} \cdot g^{-1}$		
	UiO-66-NH_2	MoS_2 quantum dots, graphene	HER	TEOA	2.0707 $mmol \cdot h^{-1} \cdot g^{-1}$		[113]
	UiO-66-NH_2	graphene	HER	TEOA	0.022 $mmol \cdot h^{-1} \cdot g^{-1}$		
Metal nanoparticles loading	NH_2-MIL-101(Cr)	Pt NPs	HER	TEOA	≈0.583 $mmol \cdot h^{-1} \cdot g^{-1}$	5	[56]
	UiO-66-NH_2	Pt NPs (incorporated inside MOF)	HER	TEOA	0.25738 $mmol \cdot h^{-1} \cdot g^{-1}$	4	[123]
	UiO-66-NH_2	Pt NPs (supported on MOF)	HER	TEOA	0.05026 $mmol \cdot h^{-1} \cdot g^{-1}$		
	MIL-125(Ti)	Pt NPs (Ti^{3+} assisted method)	HER	TEOA	0.15472 $mmol \cdot h^{-1} \cdot g^{-1}$		[125]
	MIL-125(Ti)	Pt NPs (photodeposition method)	HER	TEOA	≈0.08 $mmol \cdot h^{-1} \cdot g^{-1}$		
	NH_2-MIL-125(Ti)	$Ni_{15.8}Pd_{2.1}$ NPs	HER	TEOA	8.7 $mmol \cdot h^{-1} \cdot g^{-1}$	3	[94]
	UiO-66	Ni_2P NPs	HER	TEOA	2 $mmol \cdot h^{-1} \cdot g^{-1}$	4	[127]
	NH_2-MIL-125(Ti)	Ni_2P NPs	HER	TEA	0.894 $mmol \cdot h^{-1} \cdot g^{-1}$	7	[128]
	NH_2-MIL-125(Ti)	Pt NPs	HER	TEA	≈0.269 $mmol \cdot h^{-1} \cdot g^{-1}$		
	UiO-66-NH_2	NiO NPs	HER	TEOA	2.56132 $mmol \cdot h^{-1} \cdot g^{-1}$	3	[129]
	UCNPs-Pt@MOF/Au (under NIR light)	UCNPs, Pt NPs, Au NPs	HER	TEOA	0.280 $mmol \cdot h^{-1} \cdot g^{-1}$	4	[126]
	Cd-TBAPy	Pt NPs	HER	TEOA	0.086 $mmol \cdot h^{-1} \cdot g^{-1}$		[124]
	Cd-TBAPy	CoPi NPs	OER	$AgNO_3$	1.634 $mmol \cdot h^{-1} \cdot g^{-1}$		
Sensitization	MIL-101(Cr),	Erythrosin B	HER	TEOA	6.25 $mmol \cdot h^{-1} \cdot g^{-1}$		[131]
	UiO-66	Erythrosin B(30 mg)	HER	l-ascorbic acid	0.46 $mmol \cdot h^{-1} \cdot g^{-1}$	3	[132]
	UiO-66-NH_2	cone-calixarene-based dye (200 ppm $CHCl_3$ solution)	HER	methanol	1.528 $mmol \cdot h^{-1} \cdot g^{-1}$	3	[133]
	MIL-101(Cr)	$[Ru(bpy)_3]^{2+}$	HER	TEOA	25.578 $mmol \cdot h^{-1} \cdot g^{-1}$		[134]
	MIL-101(Fe)	$[Ru(bpy)_3]^{2+}$	HER	TEOA	21.732 $mmol \cdot h^{-1} \cdot g^{-1}$		
	MIL-101(Al)	$[Ru(bpy)_3]^{2+}$	HER	TEOA	27.082 $mmol \cdot h^{-1} \cdot g^{-1}$		
Incorporation of polyoxometalates (POM)	SMOF-1	Wells-Dawson-type POM	HER	methanol	3.353 $mmol \cdot h^{-1} \cdot g^{-1}$		[138]
	MIL-101(Cr)	$[Co_4(H_2O)_2(PW_9O_{34})_2]^{10-}$ POM	OER	$Na_2S_2O_8$	≈6.7 $mmol \cdot h^{-1} \cdot g^{-1}$		[139]
	MIL-100(Fe)	$[Co_4(H_2O)_2(PW_9O_{34})_2]^{10-}$ POM	OER	$Na_2S_2O_8$	≈7.5 $mmol \cdot h^{-1} \cdot g^{-1}$		[140]
	MOF-545	$[Co_4(H_2O)_2(PW_9O_{34})_2]^{10-}$ POM	OER	$Na_2S_2O_8$	≈4 $mmol \cdot h^{-1} \cdot g^{-1}$	3	[141]
	$[Ir(ppy)_2(bpy)]^+$-derived UiO-MOF	$[Ni_4(H_2O)_2(PW_9O_{34})_2]^{10-}$ POM	HER	methanol	4.4 $mmol \cdot h^{-1} \cdot g^{-1}$	3	[142]

*If not stated, the light source of photocatalyst refers to visible light.

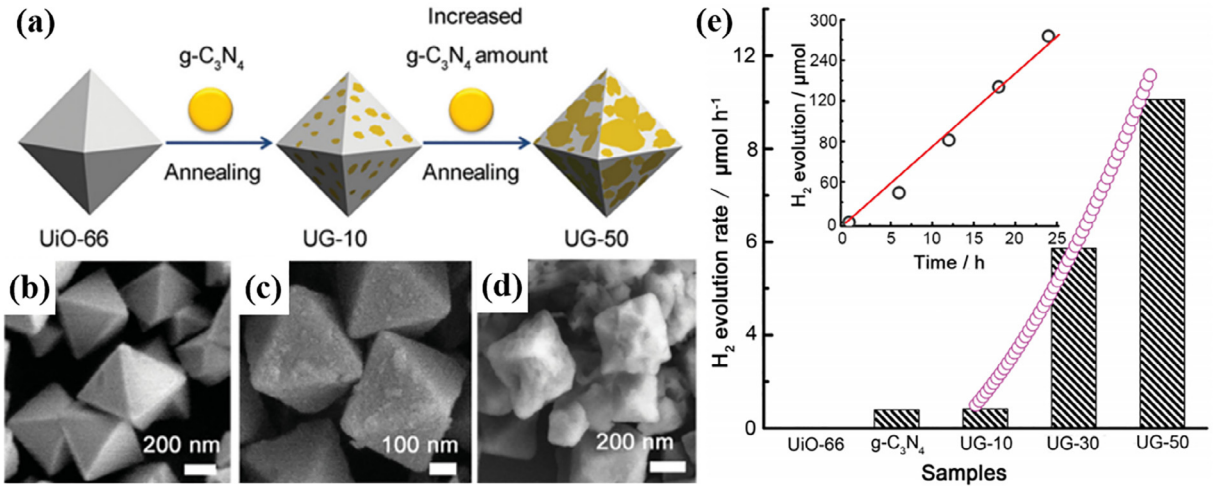

Fig. 5. (a) Schematic illustration of decorating g-C_3N_4 on UiO-66 octahedrons through annealing process. SEM images of (b) UiO-66, (c) UG-10 and (d) UG-50. (e) The histogram showing the hydrogen production rate over pristine UiO-66, g-C_3N_4 and UG-x samples (x = 10, 30, and 50), the inset shows the long term hydrogen production over UG-50 sample (UG-x means UiO-66 and g-C_3N_4 composites and x is the mass content of g-C_3N_4 in hybrids). Reprinted with the permission from Ref. [90]. Copyright 2015 Wiley.

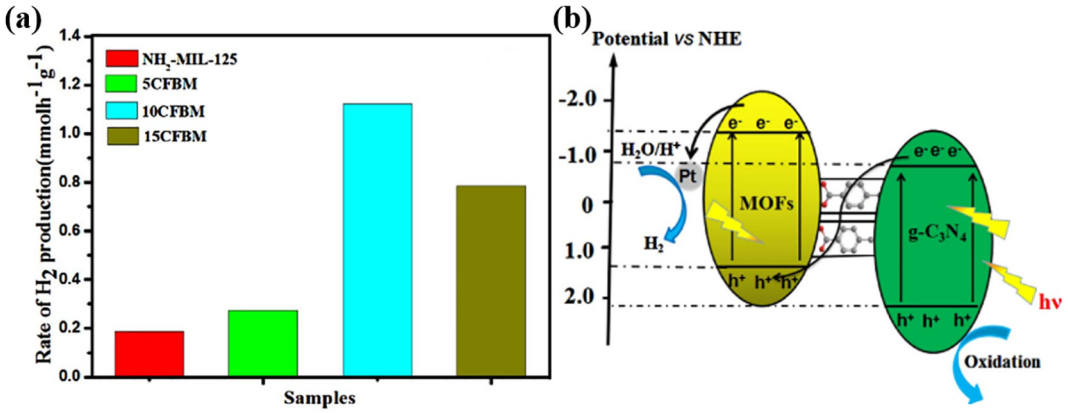

Fig. 6. (a) The rate of hydrogen evolution of NH_2-MIL-125, 5CFBM, 10CFBM and 15CFBM under visible light irradiation. (b) Photocatalytic mechanism of the charge transfer for hydrogen evolution over the 10CFBM under visible light irradiation. Reprinted with the permission from Ref. [92]. Copyright 2018 Elsevier.

the amount of hydrogen generation dropped significantly when mass fraction of g-C_3N_4 in hybrid was 70%, which was ascribed to the "covering effect". Recently, ultrathin two-dimensional meta-organic framework (UMOF) nanosheets have aroused numerous attentions. Cao et al. have attempted to assemble 2 dimentional (2D) g-C_3N_4 nanosheets and 2D Ni-based MOF nanosheets together by self-assembly process [91]. Benefiting from the ultrathin thickness of 2D structure, the electrons transfer more efficiently and further boost the photocatalytic efficiency. In addition to changing the morphology of the composite, employing organic acids as an electronic mediator can also strengthen the photocatalytic performance. For instance, NH_2-MIL-125(Ti) MOF have been combined with benzoic acid functionalized graphitic carbon nitride (g-C_3N_4) to build a Z-scheme heterojunction photocatalyst for HER [92], in which semiconductor and MOF were connected by covalent bonds as the carboxylate groups of the functionalized g-C_3N_4 are coordinated with the Ti ions of MOF. More than promote suitable heterojunction formed, the benzoic acid also acts as electron mediator to induce recombination of holes in MOF and electrons in g-C_3N_4 (Fig. 6b), leading to high hydrogen generation rate of 1.123 mmol·h^{-1}·g^{-1} that equivalent to 6 times of pristine NH_2-MIL-125(Ti) MOF (Fig. 6a). After four cycles, the photocatalytic H_2 evolution rate of 10 wt%g-C_3N_4/MOFs was markedly reduced by 0.1 mmol·h^{-1}·g^{-1}. In contrast, the photocatalytic H_2 evolution rate of novel MOFs nearly became unchanged. This explains that the novel Z-scheme heterostructured catalysts linked by covalent bonds shows better water stability than the conventional 10 wt%g-C_3N_4/MOFs linked by van der Waals force. Moreover, the amine group of g-C_3N_4 makes it possible to anchor metal nanoparticles [93]. Bimetal nanoparticles NiPd NPs were also introduced into MOF/g-C_3N_4 photocatalytic systems as co-catalyst [94]. The strong light-harvesting abilities of NiPd NPs were beneficial to improve photocatalytic performance of MOF/g-C_3N_4. As a result, the photocatalytic hydrogen production rate of NH_2-MIL-125(Ti)/0.75 g-C_3N_4/$Ni_{15.8}Pd_{2.1}$ was about 322 times than that of NH_2-MIL-125(Ti)/0.75 g-C_3N_4.

Owing to its ideal band gap (2.4 eV) and excellent photoelectric properties [95], CdS NPs also have been encapsulated into MOFs, such as MIL-101(Cr) [96] and UiO-66 [97], to provide extra active sites. However, these composites also bring some severe challenges, for example, the photogenerated electrons and holes are easily recombined. To solve this problem, a ternary complex Au@CdS/MIL-101 has been synthesized by deposited Au nanoparticles on the MIL-101 and CdS coated on Au nanoparticles subsequently [98], and the outstanding catalytic capacity of the as-synthesized ternary complex (hydrogen production rate: 25 mmol·h^{-1}·g^{-1}) could ascribe to two aspects: (i) Au accelerate charge transition and enlarge the visible light response spectrum of CdS, (ii) MOF not only serve as support to disperse nanoparticles but generate electrons under light irradiation. Recently, carbon nanodots (CDs) particles have been introduced into MIL-

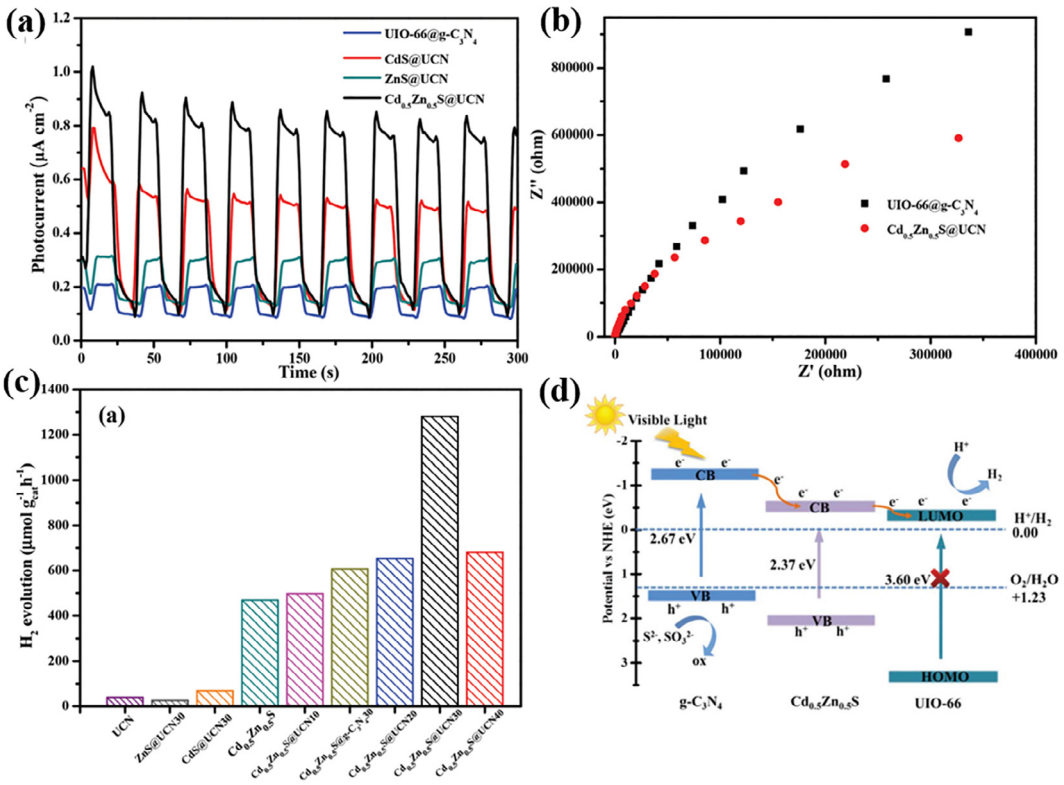

Fig. 7. (a) Transient photocurrent response of the UiO-66@g-C_3N_4, ZnS@UiO-66@g-C_3N_4, CdS@UiO-66@g-C_3N_4 and $Cd_{0.5}Zn_{0.5}S$@UiO-66@g-C_3N_4 under visible-light irradiation. (b) The EIS Nyquist plots of the UiO-66@g-C_3N_4 and $Cd_{0.5}Zn_{0.5}S$@UiO-66@g-C_3N_4 composites. (c) Photocatalytic hydrogen evolution rate under visible light irradiation over the as-prepared samples (Na_2S and Na_2SO_3 were used as the hole scavenger without noble metal co-catalysts). (d) Schematic of photocatalytic hydrogen evolution over the $Cd_{0.5}Zn_{0.5}S$@UiO-66@g-C_3N_4 under visible light irradiation. Reprinted with the permission from Ref. [101]. Copyright 2018 Royal Society of Chemistry.

101@CdS system for further promoting charge transfer efficiency [99]. The prolonged lifetime of electrons of CD/CdS@MIL-101 also contribute to enhance photocatalytic hydrogen evolution activity. Additionally, be endowed with higher photoactivity than pure CdS, binary metal sulfide $Cd_{0.5}Zn_{0.5}S$ aroused numerous attention [100]. For instance, $Cd_{0.5}Zn_{0.5}S$ has been introduced into UiO@g-C_3N_4 (denoted as UCN) system to construct a ternary heterojunction (Fig. 7d) [101], and the photocurrent intensity improved from 0.20 μA cm^{-2} of UCN to 0.82 μA cm^{-2} of $Cd_{0.5}Zn_{0.5}S$@UCN (Fig. 7a), which demonstrated more photoelectrons generation of UCN after $Cd_{0.5}Zn_{0.5}S$ decoration. Meanwhile, the electrochemical impedance spectra (EIS) Nyquist plots proved higher electrical conductivity of $Cd_{0.5}Zn_{0.5}S$@UCN than UCN as the arc radius of $Cd_{0.5}Zn_{0.5}S$@UCN was smaller (Fig. 7b). Accordingly, the hydrogen production activity of $Cd_{0.5}Zn_{0.5}S$@UCN enhanced significantly than other counterparts (Fig. 7c).

Likewise, other semiconductors such as MoS_2 and Cu_2O also have been explored for combination with MOFs. MoS_2 composed of a layered structure has been widely investigated because of its high activity for solar hydrogen production [102]. For example, MoS_2 has coupled with UiO-66/CdS system and serves as one kind of noble-metal-free co-catalyst for HER in visible light [103]. Since the well-matched band structures of three components, the ternary heterojunction presented remarkable hydrogen production rate, i.e. 32.5 mmol·h^{-1}·g^{-1}, which is better than the ternary heterojunction that Pt as co-catalyst. Besides, as an economical and sustainable semiconductor, Cu_2O has also been applied in photocatalytic hydrogen evolution by post-synthetic encapsulation into NH_2-MIL-125(Ti) [104]. Specifically, the Ti^{4+} of NH_2-MIL-125(Ti) partially reduced to Ti^{3+} during post-synthetic encapsulation, and the increased hydrogen evolution could be ascribed to the efficient charge separation between Cu_2O and Ti^{3+}. More recently, traditional semiconductor TiO_2 hollow nanospheres (TiO_2 HNPs) have been created through template method and then decorated by ZIF-8 MOFs [105], the photocatalytic performance of this heterogeneous photocatalyst promoted greatly because the shell of TiO_2 HNPs enlarged the surface area.

3.2.2. Decoration of graphene

Graphene is a single-layer carbon atom-plane material which is stripped from graphite materials [106]. It shows superior thermal and electrical conductivity, high chemical stability. Especially graphene oxide (GO) and reduced GO (rGO) are widely studied and applied [107]. GO can facilitate charges transfer and surface-adsorbed number of chemical molecules through π–π interactions. MOFs could potentially evolve into highly efficient photocatalysts when incorporated into graphene decorated system. In the photocatalytic system, the GO serves as electron-transfer mediator, provides more active sites and leads to significantly improvement of the photo-generated charge separation efficiency [108]. Wang et al. introduced GO to UiO-66-NH_2 by applying three incorporation methods respectively, i.e. random mixing, single-face interaction and multiple-face interaction [109], and the results manifested that every face of UiO-66-NH_2 MOF was covered by GO and reached high hydrogen production rate (41.4 mmol·h^{-1}·g^{-1}) when employed the multiple-face interaction approach, which can be explained by the efficient charge transmission between UiO-66-NH_2 MOF and GO. Furthermore, Liu et al. not only prepared UiO-66/rGO by solvothermal method but introduced Ni_4S_3 into UiO-66/rGO by hydrothermal method to construct rGO/MOF/Ni_4S_3 photocatalytic system [110], as they expected, the light adsorption edge of rGO/MOF/Ni_4S_3 has showed significant red shift. Moreover, the hydrogen amount of EY-sensitized rGO/MOF/Ni_4S_3 photocatalyst produced about 185 times than the pure rGO/MOF photocatalyst. Besides, Shi et al. demonstrated that Cu-benzene-1,3,5-tricarboxylate (BTC) MOF could act as

microcontainer which encapsulate and stabilize the free radicals during photocatalytic reaction by electron spin resonance (ESR) analysis [111], and they incorporated it into ZnO/GO by electrostatic interaction for increasing the possibilities of H· radical recombination. Finally the photocatalytic hydrogen production amount was increased by about 9 times. Moreover, UiO-66/CdS/RGO composite has been designed to inhibit the electron-hole pairs recombination and increase more catalytic sites of CdS [112]. Likewise, the synergistic effect of GO and MoS_2 quantum dots on the photocatalytic hydrogen production of MOF also has been proved [113]. To be specific, the hydrogen generation amount of MoS_2/UiO-66-NH_2/GO reached 186.37 μmol while the UiO-66-NH_2/MoS_2 and the UiO-66-NH_2/GO was 75.1 μmol and 1.98 μmol, respectively.

3.2.3. Metal nanoparticles loading

Nanotechnology has developed rapidly and is widely used in medicine, biology and biochemical engineering in recent years [114,115]. Also, the inherent advantages of nanomaterials such as various morphologies and abundant surface states make a new path for the use of renewable energy [116,117]. Metal nanoparticles (MNPs) is a kind of excellent catalyst compared with the bulk noble metals, which reflected in its high ratio of surface area to volume [118]. When the size of the metal particles is reduced to the order of nanometers, the catalytic performance of MNPs will improve significantly [119,120]. However, MNPs is tended to aggregate with each other in solution and greatly suppressed its catalytic property [121]. To prevent this phenomenon, stable supports such as MOFs are utilized for MNPs dispersion, meanwhile MNPs serve as co-catalyst for efficient spatial charge separation.

Noble MNPs have attracted numerous attention in catalysis due to their outstanding catalysis behavior [122]. Notably, Pt NPs have been frequently applied with MOF for photocatalytic water splitting. Wen et al. constructed a Pt NPs loaded and RhB sensitized NH_2-MIL-101(Cr) for HER, significantly improved the efficiency of electron-hole separation [56]. Moreover, the influence of different Pt NPs spatial position on the photocatalytic activity of UiO-66-NH_2 also have been investigated [123], and the results indicated that UiO-66-NH_2 encapsulated Pt NPs into pores showed higher efficiency of charge separation than UiO-66-NH_2 that supported Pt NPs on the surface. Besides, Pt NPs confined in pores are less likely to leak or aggregate than deposited on the surface. Recently, a novel Cd-based MOFs (denoted as Cd-TBAPy) has been reported [124], the novel Cd-TBAPy possess excellent solvent and thermal stability and ideal band gap of 2.15 eV for visible light adsorption as well as sufficient potential of both VB and CB for water oxidation and reduction (Fig. 8), simultaneously realized effective HER and OER after loading Pt and CoPi co-catalyst. Particularly, a novel approach has been reported that through a redox reaction between oxidative metal salt and reductive Ti^{3+}-MIL-125(Ti) to decorate MIL-125(Ti) with noble M (Pt, Pd and Au NPs) [125]. The as-synthesized Pt/MIL-125(Ti) showed a higher hydrogen amount (38.68 μmol) than the Pt/MIL-125(Ti) (about 20 μmol) prepared by photodeposition method. Au NPs with excellent catalytic properties can also be applied in photocatalysis. Interestingly, Jiang et al. have extended the spectral response range of MOFs to NIR light by constructing core-shell structure UCNPs-Pt@MOF/Au composites (UCNPs denote $NaYF_4$:Yb, Tm, Er) [126]. In this composite, UCNPs could accept NIR light and convert it into ultraviolet and visible light that could be further utilized by MOF and Au NPs. In this case, UCNPs-Pt@MOF/Au showed excellent catalysis activity for hydrogen evolution under stimulated solar light.

In recent work, noble metal nanoparticles have been replaced or partial replaced by earth-abundant metals for clean energy technology. Nickel (Ni) based co-catalyst received tremendous attention because of its excellent catalysis activity for photocatalytic application. For instance, Ni has been incorporated with noble metal palladium (Pd) to construct NiPd co-catalyst for hydrogen production [94]. Ni_2P NPs are also inserted into g-C_3N_4/UiO-66 system to inhibit recombination of electrons and holes (Fig. 9) [127]. Accordingly, the hydrogen evolution rate of g-C_3N_4/UiO-66/Ni_2P is higher than g-C_3N_4/UiO-66. Additionally, the photocatalytic performance of NH_2-MIL-125(Ti)/Ni_2P and NH_2-MIL-125(Ti)/Pt has been compared for HER in visible light [128]. The photocurrent response and the photoluminescence spectrum (PL) showed that NH_2-MIL-125(Ti)/Ni_2P performed higher efficient electron transfer and lower possibility of recombination than Pt/NH_2-MIL-125(Ti). Recently, p-type semiconductor NiO co-catalyst, which worked as collector of photogenerated electrons, has been embedded in UiO-66-NH_2 and this composite showed enhanced hydrogen production rate of 2561.32 $\mu mol \cdot h^{-1} \cdot g^{-1}$ [129].

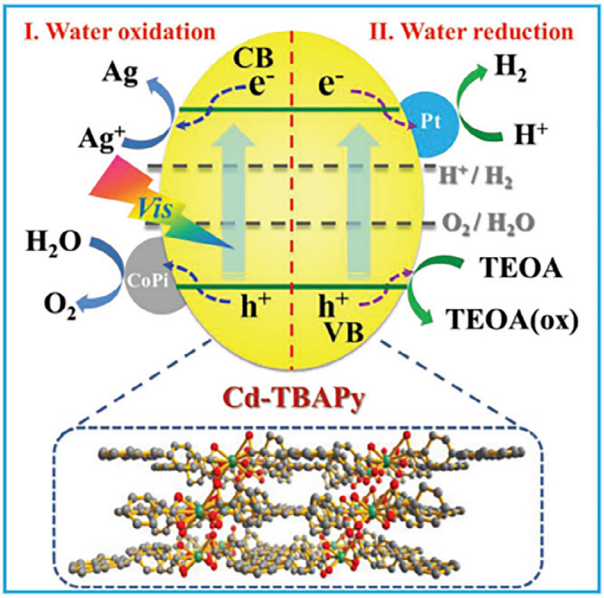

Fig. 8. The proposed mechanism for visible-light-driven photocatalytic hydrogen and oxygen evolution over Cd-TBAPy. Reprinted with the permission from Ref. [124]. Copyright 2018 Wiley.

3.2.4. Sensitization

Besides loading metal nanoparticles, dye-sensitization is another appealing approach to boost the photocatalytic efficiency. Dye-sensitization has been widely used in the field of semiconductors, and has been gradually regarded as an effective strategy to enhance the photocatalytic performance of MOFs for water splitting. Between MOF and organic dye, various forces (such as π-π interaction and Van der Waals force) could effectively suppress the recombination of photogenerated electrons and holes, which benefit for photocatalytic reaction [129]. RhB has been combined with MOF for hydrogen production [56]. Nevertheless, RhB is not a suitable photosensitizer since its poor stability for photocatalytic application [130]. Conversely, erythrosin B (ErB) is a kind of relatively stable dye and has been used for improving the photocatalytic performance of MOF. Liu et al. applied ErB as photosensitizer to sensitize MIL-101 which loaded Ni/NiO_x NPs [131]. The results unveiled that moderate amount of ErB dye could effectively facilitate hydrogen generation, but excessive amount lead to competition between ErB dyes and resulted in low hydrogen evolution rate. Similarly, Yuan et al. employed UiO-66 which was sensitized by ErB dye and deposited by Pt NPs for hydrogen production in visible light [132]. As for dye and MOF combination system, efficient electron transfer and high hydrogen production rate mostly depended on the stability of dye and MOF binding. For instance, a cone-calixarene-based dye (denoted as Calix-3) has been used as light absorbing antenna of UiO-66-NH_2/Pt system for HER [133]. Except from Van der Waals force and π-π stacking, hydrogen bond among Calix-3 dye and UiO-66-NH_2 MOF also have influence on their stability. It was indicated that small amount $-NH_3^+$ groups of UiO-66-NH_2 has strong binding with –COOH

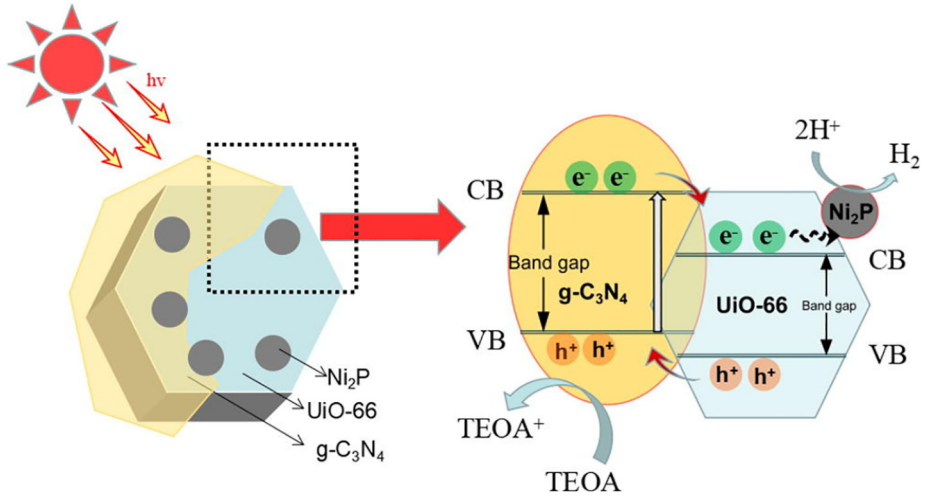

Fig. 9. Schematic for the mechanism of g-C_3N_4/UiO-66/Ni_2P photocatalytic hydrogen production. Reprinted with the permission from Ref. [127]. Copyright 2018 Elsevier.

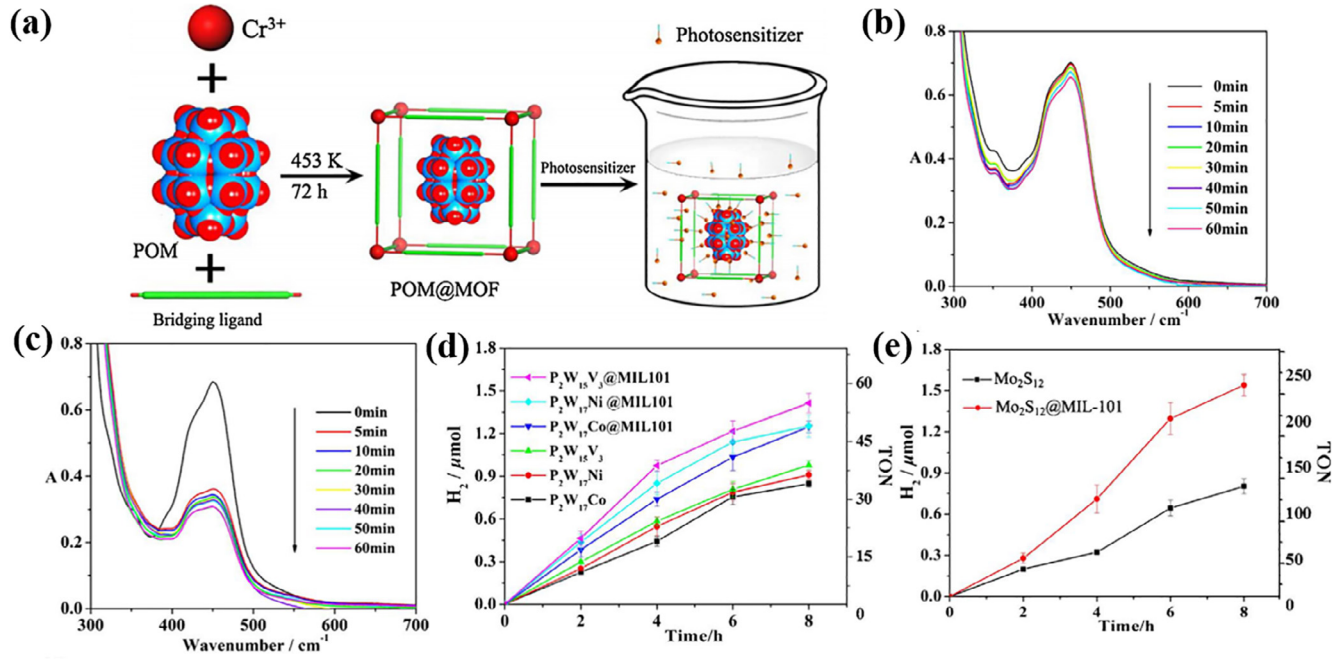

Fig. 10. (a) Scheme view for constructing POM@MOF and POM@Photosensitizer@MOF composite materials. UV–vis spectra of $[Ru(bpy)_3]^{2+}$ (48 μM) solution in the presence of 10 mg (b) isolated MIL-101 and (c) MIL-101 and 80 mg $P_2W_{15}V_3$. (d) Kinetics of hydrogen production in the photocatalytic system with different catalysts. (e) Kinetics of hydrogen production in the photocatalytic system with Mo_2S_{12}. Reprinted with the permission from Ref. [134]. Copyright 2018 Elsevier.

moieties of Calix-3 dye and lead to higher hydrogen production rate. Recently, Li et al. reported a novel and simple manner for constructing a photoactive MIL-101(Cr) with polyoxometalates (POMs) loaded and $[Ru(bpy)_3]^{2+}$ sensitized [134], i.e. introduced the anionic POMs into cationic MOF that could overcompensated the charge of MIL-101(Cr), and then the anionic MIL-101(Cr)@POM composites absorbed cationic $[Ru(bpy)_3]^{2+}$ from solution (Fig. 10a). It has been proved that MOF@$P_2W_{15}V_3$ POM showed better light adsorption activity than isolated MIL-101(Cr) (Fig. 10b and c). Therefore, the performance of photocatalytic hydrogen production of MIL-101(Cr) corporated with different POMs was higher than homogeneous photocatalytic system (Fig. 10d and e).

3.2.5. Incorporation of polyoxometalates (POM)

Polyoxometalates (POM) is a class of inorganic polyatomic clusters formed by linking transition metal atoms with oxygen atoms. POM owns excellent redox ability, various structural characteristics and highly negative charges, playing a vital role in catalytic reaction. Particularly, POM has been widely utilized in water-splitting half reaction as it could maintain its structure during intricate electron transfer [135]. However, POM also restrict its catalytic application by small surface area and low stability in aqueous solution [136]. Immobilization of POMs into MOFs has been demonstrated to be a promising approach to optimize the catalytic performance and the structure stability of MOFs. The interactions between the function group of MOFs and POMs dramatically improved catalytic activity. The synergistic effect enhances the stability of both components mutually. For instance, POM ($H_3PW_{12}O_{40}$) and Pt NPs have been encapsulated into NH_2-MIL-53 [137], in which POM not only stabilized Pt NPs onto the surface of NH_2-MIL-53 MOF but promoted photocatalytic water reduction. At the same time, a polycationic supramolecular MOF (SMOF-1) has been fabricated, and SMOF-1 which adsorbed anionic Wells-

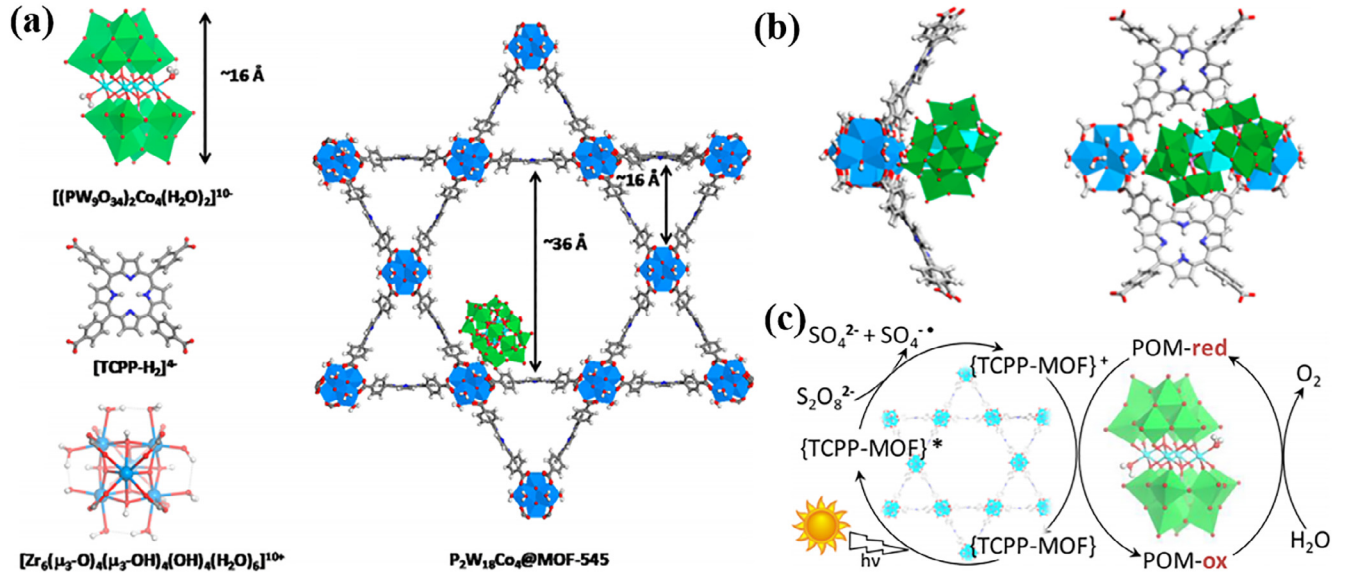

Fig. 11. (a) Systematic illustration of $[Co_4(H_2O)_2(PW_9O_{34})_2]^{10-}$ POM, TCPP-H_2 linker, Zr-based unit and $P_2W_{18}Co_4$@MOF-545. (b) Computed position of the $P_2W_{18}Co_4$ POM in MOF-545, "Side" (left) and "top" (right) views of the POM positioned between two Zr_6-clusters and two porphyrins. (c) Schematic representation of the proposed mechanism for the light-driven OER by $P_2W_{18}Co_4$@MOF-545. Adapted and reprinted with the permission from Ref. [141]. Copyright 2018 American Chemical Society.

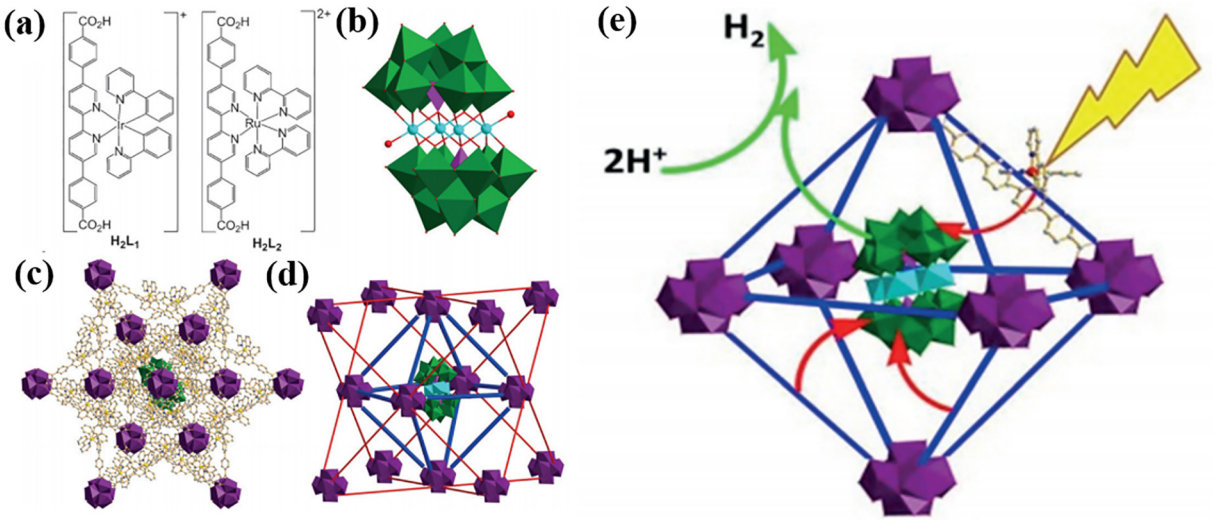

Fig. 12. (a) Chemical structures of $[Ir(ppy)_2(bpy)]^+$-derived dicarboxylic acid and $[Ru(bpy)_3]^{2+}$-derived dicarboxylic acid. (b) Polyhedral view of the structure of $[Ni_4(H_2O)_2(PW_9O_{34})_2]^{10-}$ POM. (c) Structural model of $[Ni_4(H_2O)_2(PW_9O_{34})_2]^{10-}$ POM@MOF as viewed along the [1, 1, 1] direction. (d) Structural model showing unoccupied tetrahedral cavities and the central $[Ni_4(H_2O)_2(PW_9O_{34})_2]^{10-}$ POM-loaded octahedral cavity. (e) Schematic showing the injection of electrons to the $[Ni_4(H_2O)_2(PW_9O_{34})_2]^{10-}$ POM upon photoexcitation of the MOF framework to enable proton reduction. Reprinted with the permission from Ref. [142]. Copyright 2016 Wiley.

Dawson-type POM also exhibited efficient hydrogen production rate [138]. Co-based POM which contain earth abundant element has well catalytic properties for water oxidation. As one of the most typical Co-based POM, $[Co_4(H_2O)_2(PW_9O_{34})_2]^{10-}$ has been introduced into MIL-101(Cr) by an ion exchange method [139]. The synergistic effect between MIL-101(Cr) and Co-POM enhanced the photoactivity of this composite than single-component. However, due to the large window sizes of MIL-101(Cr), the Co-POM in the pores of MIL-101(Cr) will leak away and lost its activity. Accordingly, a more appropriate host MIL-100(Fe) MOF has been investigated to immobilize $[Co_4(H_2O)_2(PW_9O_{34})_2]^{10-}$ POM and further applied in water oxidation reaction [140]. The results suggested that the TOF and oxygen yield of MIL-100(Fe)/Co-POM ($9.2 \times 10^{-3}\,s^{-1}$; 72%) were higher than MIL-101(Cr)/Co-POM ($7.3 \times 10^{-3}\,s^{-1}$; 66%). MOF-545 which consisted of Zr-based clusters and TCPP-H_2 linker has been fabricated [141] (Fig. 11a and b). Different from previous studies that used noble metal composites as photosensitizer, MOF-545 inherited photoactivity from the TCCP-H_2 linker which could adjust the valence band. After encapsulated $[Co_4(H_2O)_2(PW_9O_{34})_2]^{10-}$ POM into channels, MOF-545 also possessed Co-POM as catalyst for efficient water oxidation (Fig. 11c). Besides, Kong et al. embedded $[Ni_4(H_2O)_2(PW_9O_{34})_2]^{10-}$ POM into $[Ir(ppy)_2(bpy)]^+$-derived (ppy = 2-phenylpyridine) and $[Ru(bpy)^3]^{2+}$-derived UiO-MOF (Fig. 12a–d), respectively [142], which indicated that Ir-based UiO-MOF exhibited highly photocatalytic performance for HER than the Ru-based UiO-MOF, and the mechanism was similar to Co-POM/MOF for OER (Fig. 12e).

Table 3
Photocatalytic performance of MOFs derivatives.

Strategies	Photocatalysts	Template of MOF	Pyrolysis temperature	Target reaction	Sacrificial reagent	Production rate ($mmol \cdot h^{-1} \cdot g^{-1}$)	Recycled times	Ref.
Pyrolyzation	N-doped graphene analogs	ZIF-8	1000 °C	HER	TEOA	0.37 $mmol \cdot h^{-1} \cdot g^{-1}$	4	[156]
	ZnO/Co_3O_4	ZnCo-ZIF	350 °C	HER	methanol	7.80 $mmol \cdot h^{-1} \cdot g^{-1}$	5	[149]
	Au/ZnO	glutathione-Au nanoclusters/ZIF-8	550 °C	HER	Na_2S and $NaSO_3$	0.0298 $mmol \cdot h^{-1} \cdot g^{-1}$	4	[147]
	ZnO	ZIF-8	550 °C	HER	Na_2S and $NaSO_3$	1×10^{-5} $mmol \cdot h^{-1} \cdot g^{-1}$		
	C-ZIF/g-C_3N_4	ZIF-8 (melamine)	650 °C	HER	TEOA	0.0326 $mmol \cdot h^{-1} \cdot g^{-1}$	4	[157]
	ZnO/rGO/carbon sponge	ZIF-8/GO/melamine foam	350 °C	HER	methanol	0.0146 $mmol \cdot h^{-1} \cdot g^{-1}$	3	[150]
	ZnO/carbon sponge	ZIF/melamine foam	350 °C	HER	methanol	0.0134 $mmol \cdot h^{-1} \cdot g^{-1}$		
	Hierarchical TiO_2	NH_2-MIL-125(Ti)	400 °C	HER	methanol	48.985 $mmol \cdot h^{-1} \cdot g^{-1}$ (UV–vis light)		[151]
	CN/FeNiP (co-catalyst)	NH_2-MIL-101(Fe)/$Ni(OH)_2$	350 °C	HER	TEOA	13.81 $mmol \cdot h^{-1} \cdot g^{-1}$	5	[161]
	CN/FeP (co-catalyst)	NH_2-MIL-101(Fe)	350 °C	HER	TEOA	2.73 $mmol \cdot h^{-1} \cdot g^{-1}$		
	Fe_2O_3	MIL-88B/GO	600 °C	HER	TEA	0.318 $mmol \cdot h^{-1} \cdot g^{-1}$ (Xe lamp irradiation)	4	[153]
	HP-CdS	MIL-53(Al)/CdO	350 °C	HER	Na_2S and $NaSO_3$	0.63 $mmol \cdot h^{-1} \cdot g^{-1}$	4	[159]
	Ni_2P (co-catalyst)	Ni-BTC MOF	275 °C	HER	lactic acid	33.48 $mmol \cdot h^{-1} \cdot g^{-1}$	5	[162]
	NiS/$Zn_{0.5}Cd_{0.5}S$	Ni-Zn_xCd_{1-x}-MOF	580 °C	HER	Na_2S and $NaSO_3$	16.78 $mmol \cdot h^{-1} \cdot g^{-1}$	5	[160]
	Co_3O_4/CuO	ZIF-67/$Cu(NO_3)_2 \cdot 6H_2O$	360 °C	OER	$Na_2S_2O_8$	0.01244 mmol (0.2 g L^{-1} catalyst after 11 min photoirradiation)	5	[148]

* If not stated, the light source of photocatalyst refers to visible light.

4. MOF derivatives as photocatalysts

As a highly ordered porous crystalline catalyst with periodical structure, MOFs have been widely employed as sacrificial template or precursor to prepare porous materials (such as porous carbon and metal oxides) by calcination process [144,145]. The resulting derivatives can largely maintain the initial structures and typologies feature of parent MOFs, and possess dispersed nanoscale subunits, rich active sites and high surface area [146]. These merits have motivated the attempt to utilize MOFs derivatives for photocatalytic application, and the recent developments of MOFs derivatives for HER and OER are summarized in Table 3.

4.1. Metal oxides

Among various MOF materials, ZIFs have been explored widely due to its excellent thermal stability and water tolerance. There are many researches on metal oxides which are obtained by using ZIF as precursors. For example, Au/ZnO nanoparticles have been obtained by the calcination of glutathione-Au nanoclusters/ZIF-8 [147], and the enhanced photocatalytic performance result from the efficient charge transfer of Au/ZnO NPs and the surface plasmon resonance (SPR) of Au NPs. Another porous Co_3O_4/CuO also has been constructed by the calcination of ZIF-67/$Cu(NO_3)_2 \cdot 6H_2O$ at 360 °C [148]. The porous Co_3O_4/CuO catalysts showed excellent water oxidation performance when both photosensitizer ($[Ru(bpy)_3]^{2+}$) and electron acceptor ($Na_2S_2O_8$) were added (Fig. 13a). It can be ascribe to the heterojunction formed and the sufficient potential of the valence band of Co_3O_4/CuO to drive OER (Fig. 13b). Besides, Lan and co-workers fabricated the porous Pt-doping ZnO-Co_3O_4 heterojunctions by calcinating the bimetallic ZnCo-ZIF MOFs and depositing Pt NPs [149]. The scanning electron microscope (SEM) and transmission electron microscope (TEM) demonstrated that ZnO-Co_3O_4 maintained the polyhedral morphology of parent ZnCo-ZIF MOF even after doping Pt NPs (Fig. 14a–c). Moreover, owing to the porous structure that inherited from ZnCo-ZIF precursor and the suitable band-structure matching between ZnO (2.7 eV) and Co_3O_4 (2.52 eV) (Fig. 14e), Pt-ZnO-Co_3O_4 also exhibited better photocatalytic performance than individual Co_3O_4 (hydrogen evolution rate: 0.19 $mmol \cdot h^{-1} \cdot g^{-1}$) and ZnO (hydrogen evolution rate: 0.22 $mmol \cdot h^{-1} \cdot g^{-1}$) (Fig. 14d). Furthermore, Su et al. synthesized a ternary composites ZnO/rGO/carbon sponge by the carbonization of ZIF-8/GO/melamine foam at 350 °C [150], and the ZIF-8 derivatives have been doped with C and N during pyrolyzation process. Hence its adsorption edge shifted to visible light region. This ternary composite possesses porous structure inherited from ZnO and carbon sponge, and the efficient charge transfer between ZnO and rGO also make the porous composites capable of degrading contaminants and hydrogen evolution.

Metal oxides derive from other MOFs also have been explored for photocatalytic applications. For instance, NH_2-MIL-125(Ti) has been used as precursor to prepare hierarchical TiO_2 with exposed active sites and large special surface area [151]. Likewise, the hierarchical TiO_2 also preserved regular structure feature of NH_2-MIL-125(Ti) precursor, and the photocatalytic performance of hierarchical TiO_2 for hydrogen evolution can be enhanced by loading Pd NPs as co-catalyst. Besides, iron oxide nanomaterials could show better visible light adsorption than TiO_2 which has wider band gap [152]. Confined by the undesirable conduction band, Fe_2O_3 derived from MIL-88B(Fe) also has been explored to incorporate with rGO [153], and the synergistic effect between them reflected in the adjustment of conduction band of Fe_2O_3 and the efficient charges separation.

4.2. Porous carbonaceous materials

Except precursors for metal oxides, MOFs could also be used as sacrificial templates to construct porous carbonaceous materials.

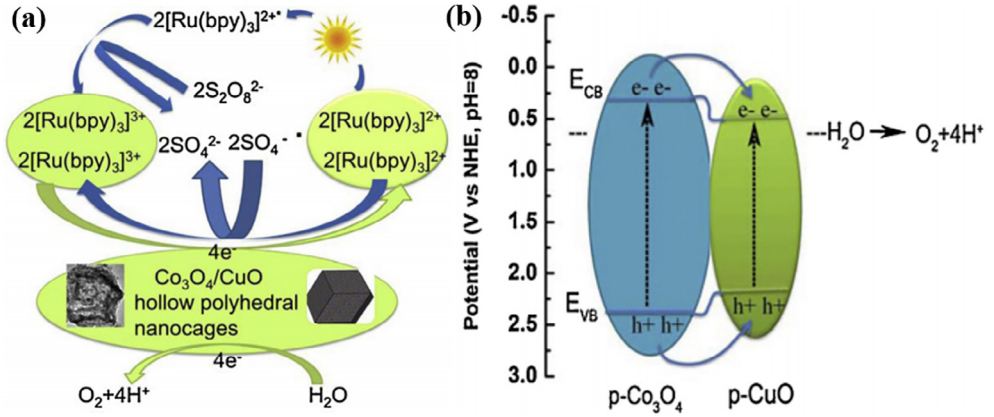

Fig. 13. (a) Photocatalytic water oxidation cycle in the presence of Co_3O_4/CuO catalyst, photosensitizer ($[Ru(bpy)_3]^{2+}$) and electron acceptor ($Na_2S_2O_8$). (b) Band diagram and mechanism of charge separation for Co_3O_4/CuO heterojunctions. Reprinted with the permission from Ref. [148]. Copyright 2016 Elsevier.

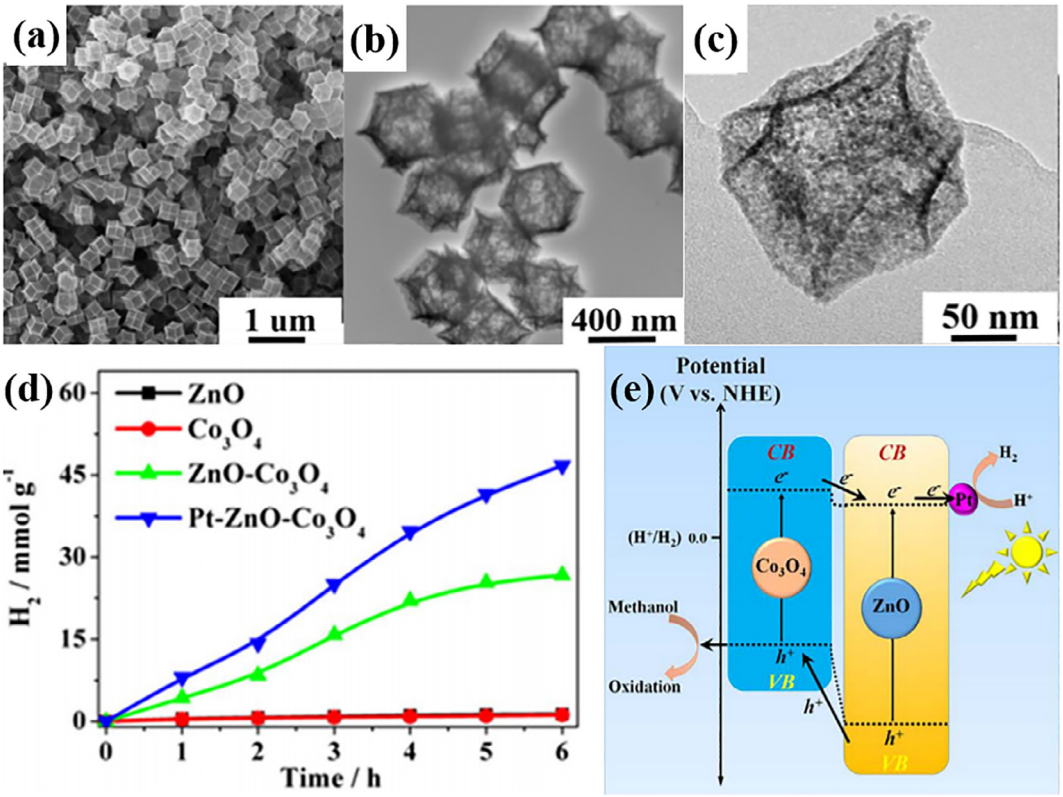

Fig. 14. (a) SEM and (b) TEM images of ZnO-Co_3O_4. (c) TEM images of Pt-ZnO-Co_3O_4. (d) Photocatalytic hydrogen generation as the function of reaction time over ZnO, Co_3O_4, ZnO-Co_3O_4, and Pt-ZnO-Co_3O_4. (e) Schematic illustration of photoexcited electron transfer and hydrogen generation over the Pt-ZnO-Co_3O_4. Reprinted with the permission from Ref. [149]. Copyright 2017 Elsevier.

Carbon nanomaterials derived from MOFs have been regarded as a promising catalyst for photocatalytic application [154,155]. For example, ZIF-8 has been calcinated under 800 °C, 900 °C and 1000 °C [156], respectively, and the formed N-doped graphene analogs almost retained unbroken structure of ZIF-8. When pyrolysis temperature was 1000 °C the derivative exhibited the highest photocatalytic efficiency for hydrogen evolution. This may be ascribed to its highest content of graphitic nitrogen, which maintains the high mobility of charges. Similarly, He et al. developed a C-ZIF/g-C_3N_4 composite by pyrolysis the mixture of ZIF-8 and melamine at 650 °C [157], and the ZIF-8 derived carbon (denoted as C-ZIF) served as co-catalyst in C-ZIF/g-C_3N_4 system for photocatalytic hydrogen production. Moreover, Zhang et al. applied an in situ calcination method to prepare porous CoO_x-carbon hybrids [158], a series of products have been fabricated by different thermal treatment of ZIF-67. Under near neutral circumstance (pH = 8.5) and $[Ru(bpy)_3]^{2+}$-$S_2O_8^{2-}$ system, CoO_x-carbon hybrids calcinated at 700 °C performed the best photocatalytic activity for OER.

4.3. Others

Templating method also could be used as effective method to prepare other porous materials. Confined by easy recombination of electrons and holes, cadmium sulfde (CdS) has been fabricated by pyrolyzation of MOFs to increase surface area. For example, Xiao et al. selected MIL-53(Al) which loaded $Cd(NO_3)_2{\cdot}4H_2O$ as sacrificial template to prepare hierarchically porous CdS [159], further enlarged the BET surface area (119 $m^2\,g^{-1}$), weakened the PL intensity, therefore improving the photocatalytic performance of CdS for hydrogen

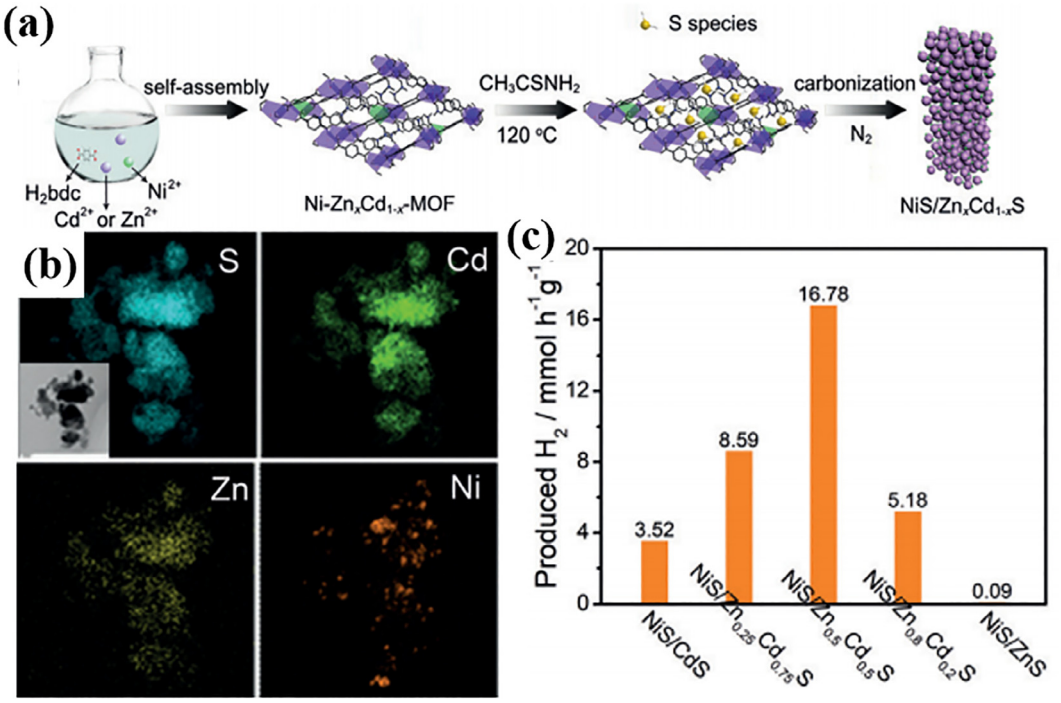

Fig. 15. (a) Schematic illustration of the synthetic procedure for NiS/$Zn_xCd_{1-x}S$. (b) EELS elemental mapping images of NiS/$Zn_{0.5}Cd_{0.5}S$. (c) Comparison of photocatalytic HER rates of NiS/$Zn_xCd_{1-x}S$ under visible-light irradiation. Reprinted with the permission from Ref. [160]. Copyright 2018 Wiley.

Table 4
Comparison of photocatalytic performance of non-MOF photocatalysts, MOFs based- and derived-photocatalysts.

	photocatalyst	HER	OER	Turnover frequency	Ref
MOF-based photocatalysts	PTC[a]/CdS/MIL-101	94.9 mmol·h^{-1}·g_{CdS}^{-1}			[143]
	Au@CdS/MIL-101	25 mmol·h^{-1}·g^{-1}			[98]
	RCGO/U6N[b]	41.4 mmol·h^{-1}·g^{-1}		161.7 h^{-1}	[109]
	Mo_2S_{12}@MIL-101(Al)	27.082 mmol·h^{-1}·g^{-1}		31.25 h^{-1}	[134]
	MoS_2/UiO-66/CdS	32.5 mmol·h^{-1}·g^{-1}			[103]
MOF-derived photocatalysts	Co_3O_4/CuO HPNCs[c]/(ZIF-67/$Cu(NO_3)_2$·$6H_2O$)		0.01244 μmol (0.2 g L^{-1} catalyst after 11 min photoirradiation)	0.2634 h^{-1}	[148]
	Pd/TiO_2/(NH_2-MIL-125(Ti))	48.985 mmol·h^{-1}·g^{-1} (UV–vis light)		40.3 h^{-1}	[151]
	Ni_2P/CdS/(Ni-BTC MOF)	33.48 mmol·h^{-1}·g^{-1}			[162]
	NiS/$Zn_{0.5}Cd_{0.5}S$/(Ni-Zn_xCd_{1-x}-MOF)	16.78 mmol·h^{-1}·g^{-1}			[160]
	Pt-ZnO-Co_3O_4/(ZnCo-ZIF)	7.80 mmol·h^{-1}·g^{-1}			[149]
	HP-CdS_d/(MIL-53(Al)/CdO)	0.63 mmol·h^{-1}·g^{-1}			[159]
The state-of-the-art non-MOF photocatalysts	CdS@NiMoS	185.4 mmol·h^{-1}·g^{-1}			[163]
	EY[e]/1T-$MoSe_2$	75.00 mmol·h^{-1}·g^{-1}		19 h^{-1}	[164]
	CoP/CdS	254 mmol·h^{-1}·g^{-1}			[165]
	Ni_2P/CdS	1200 mmol·h^{-1}·g^{-1}		36 400 h^{-1} (for Ni_2P)	[166]
	Cring–C_3N_4[f]	0.371 mmol·h^{-1}·g^{-1}	0.184 mmol·h^{-1}·g^{-1}		[167]
	Pt/Calix-3-TiO_2	2444 mmol·h^{-1}·g^{-1} (for Pt mass)		498.4 h^{-1} (for Pt)	[168]

production. Besides, Zhao et al. synthesized NiS/$Zn_xCd_{1-x}S$ catalyst by taking Cd-MOF as template (Fig. 15a) [160], and the elements of the prepared NiS/$Zn_{0.5}Cd_{0.5}S$ were homogeneously dispersed over the nanoparticles (Fig. 15b). It unveiled that different ratio of Zn to Cd resulted in different photocatalytic activity of NiS/$Zn_xCd_{1-x}S$ catalyst for hydrogen evolution (Fig. 15c). In this regard, NiS/$Zn_{0.5}Cd_{0.5}S$ achieved a good balance between ZnS which has reduction ability for hydrogen evolution and CdS which has visible light response.

Moreover, MOFs derivatives also could act as co-catalyst to replace some noble metals. Containing earth-abundant metal clusters, NH_2-MIL-101(Fe) has been cooperated with $Ni(OH)_2$ NPs as precursors for boosting the photocatalytic efficiency of g-C_3N_4 [161]. Besides, Ni_2P has been fabricated by the calcination of Ni-BTC and NaH_2PO_2 at 275 °C [162], and it could serve as co-catalyst for CdS photocatalytic system to suppress charge carrier recombination and provide active sites for proton reduction.

5. Conclusions and outlooks

Photocatalytic water splitting, including overall water spitting and water-splitting half reaction, has attracted considerable attention in energy conversion field, and it is regarded as a promising solution of energy crisis. Owning coordination-unsaturated metal sites, uniform and tailorable structure, MOFs are supposed to be an ideal

photocatalysts candidate for water splitting. In this review, recent developments of MOFs based- and derived-photocatalysts for water splitting have been summarized, and modification and decoration strategies of MOFs photocatalysts have been specifically emphasized. However, compare with other state-of-the-art non-MOF photocatalysts for HER/OER (Table 4), we could find that MOF based- and derived-photocatalysts still have space for further improvement. To be closer to industrial application, some critical issues that hamper the employment of MOFs should be taken into consideration, and future research should focus on removing these obstacles:

(1) Only few MOFs own high thermal and chemical stability, such as UiO-66 and MIL-101. Organic linkers of most MOFs will decompose under light irradiation and the structure of MOFs will collapse simultaneously, which leads to poor photocatalytic performance. Besides, since the rate of oxygen generation and hydrogen evolution is different, the pH values of aqueous photocatalytic system will fluctuate in a wide range. Consequently, it is prominent to strengthen the durability and stability of MOFs photocatalysts in acid/alkaline environment.
(2) Although surface and pore decoration strategies have greatly improved the photocatalytic performance of MOFs photocatalysts and widely applied in experiments of laboratory, there are still exist some barrier block their future industrial application. Firstly, noble metal particles co-catalysts are restricted by excessively high-cost and low recovery rate. There is still lack of research on economical and recyclable co-catalyst. Secondly, the stability of sensitized MOF by organic dye after a long operation should be given enough attention. Specifically, the type and strength of bonds between organic dyes and MOFs should discuss following routine characterization. Finally, although post-synthesize modification and decoration have applied in many researches, complicated synthesize process and harsh reaction condition make it lose its competitiveness compared to one-step method. Further exploitation of facile and effective synthesize method is also the focus of future researches.
(3) Water-splitting half reaction has been employed widely due to its less band confinement to photocatalysts. In most cases, sacrificial agents have been added into this system to consume electrons or holes, which is neither eco-friendly to water resources nor sustainable for practical application. Several researches have combined water-splitting half reaction with high-value chemicals generation by selective oxidation or reduction process to solve this problem. Reports on simultaneously generation of gas product and degradation of refractory contaminants are rare. Hence, replacing sacrificial agent with a refractory contaminant or a precursor of valuable chemical product should stimulate future works in this field.
(4) As mentioned above, sluggish oxygen evolution reaction will hamper the rate of overall water splitting. Recent reports of electrocatalysis [169,170] have replaced oxygen evolution reaction by diligent anodic reactions, which could accelerate hydrogen production rate. This also provides a solution for photocatalytic water splitting. Besides, although co-catalyst such as Pt NPs have been frequently used in water splitting system, their weak durability and high-cost make them lost competitiveness. Future works should focus on developing economical and durable cocatalysts [171]. Moreover, MOFs also have good performance in electrocatalytic energy conversion application [172], but few reports have employed MOFs in photoelectrocatalysis water splitting.
(5) Although the photocatalytic mechanism of other photocatalysts have been clearly uncovered [173], the detailed photocatalytic water splitting mechanism of MOFs is still unclear, which limited the exploration of effective MOFs photocatalysts. Therefore, rigorous experimental design and theoretical calculations are essential to fill this gap.

In summary, photocatalytic water splitting has been regarded as the realizable solution to energy crisis issue. As a class of emerging porous crystalline materials with metal clusters and organic linkers, MOFs provide possibility for modification or decoration with particular property for photocatalytic application. Despite there are still exist barriers of MOFs based- and derived-photocatalysts for water splitting application, it is expected that the recent progress will simulate more research on this field and exploit more advanced MOFs for energy conversion application.

Declaration of Competing Interest

The authors declare that they have no known competing financial interests or personal relationships that could have appeared to influence the work reported in this paper

Acknowledgements

This study was financially supported by the Program for the National Natural Science Foundation of China (51809090, 51879101, 81773333, 51579098, 51779090, 51709101, 51521006, 51278176, 51378190, 51709100, 51408206), the National Program for Support of Top-Notch Young Professionals of China (2014), the Three Gorges Follow-up Research Project (2017HXXY-05), the Program for New Century Excellent Talents in University (NCET-13-0186), the Program for Changjiang Scholars and Innovative Research Team in University (IRT-13R17), Hunan Provincial Innovation Foundation For Postgraduate (CX2018B195), and Hunan Provincial Science and Technology Plan Project (2018SK20410, 2017SK2243, 2016RS3026), the Natural Science Foundation of Hunan Province, China (Grant Nos. 2019JJ50077) and the Fundamental Research Funds for the Central Universities (531118010114, 531109200027, 531107050978).

References

[1] S. Ye, G. Zeng, H. Wu, C. Zhang, J. Dai, J. Liang, J. Yu, X. Ren, H. Yi, M. Cheng, Biological technologies for the remediation of co-contaminated soil, Crit. Rev. Biotechnol. 37 (2017) 1062–1076.
[2] X. Tang, G. Zeng, C. Fan, M. Zhou, L. Tang, J. Zhu, J. Wan, D. Huang, M. Chen, P. Xu, Chromosomal expression of CadR on Pseudomonas aeruginosa for the removal of Cd(II) from aqueous solutions, Sci. Total Environ. 636 (2018) 1355.
[3] S. Ye, G. Zeng, H. Wu, C. Zhang, J. Liang, J. Dai, Z. Liu, W. Xiong, J. Wan, P. Xu, Co-occurrence and interactions of pollutants, and their impacts on soil remediation—a review, Crit. Rev. Environ. Sci. Technol. 47 (2017) 1528–1553.
[4] C. Zhang, G. Zeng, D. Huang, C. Lai, M. Chen, M. Cheng, W. Tang, L. Tang, H. Dong, B. Huang, Biochar for environmental management: mitigating greenhouse gas emissions, contaminant treatment, and potential negative impacts, Chem. Eng. J. 373 (2019) 902–922.
[5] D. Huang, C. Hu, G. Zeng, M. Cheng, P. Xu, X. Gong, R. Wang, W. Xue, Combination of Fenton processes and biotreatment for wastewater treatment and soil remediation, Sci. Total Environ. 574 (2017) 1599–1610.
[6] C. Hu, D. Huang, G. Zeng, M. Cheng, X. Gong, R. Wang, W. Xue, Z. Hu, Y. Liu, The combination of Fenton process and Phanerochaete chrysosporium for the removal of bisphenol A in river sediments: mechanism related to extracellular enzyme, organic acid and iron, Chem. Eng. J. 338 (2018) 432–439.
[7] Y. Liu, M. Cheng, Z. Liu, G. Zeng, H. Zhong, M. Chen, C. Zhou, W. Xiong, B. Shao, B. Song, Heterogeneous Fenton-like catalyst for treatment of rhamnolipid-solubilized hexadecane wastewater, Chemosphere 236 (2019) 124387.
[8] X. Ren, G. Zeng, L. Tang, J. Wang, J. Wan, Y. Liu, J. Yu, H. Yi, S. Ye, R. Deng, Sorption, transport and biodegradation–an insight into bioavailability of persistent organic pollutants in soil, Sci. Total Environ. 610 (2018) 1154–1163.
[9] Y. Yan, T. He, B. Zhao, K. Qi, H. Liu, B.Y. Xia, Metal/covalent-organic frameworks-based electrocatalysts for water splitting, J. Mater. Chem. A 6 (2018) 15905–15926.
[10] D. Huang, S. Chen, G. Zeng, X. Gong, C. Zhou, M. Cheng, W. Xue, X. Yan, J. Li, Artificial Z-scheme photocatalytic system: what have been done and where to go? Coord. Chem. Rev. 385 (2019) 44–80.
[11] A. Fujishima, K. Honda, Electrochemical photolysis of water at a semiconductor electrode, Nature 238 (1972) 37.
[12] Y. Fang, Y. Ma, M. Zheng, P. Yang, A.M. Asiri, X. Wang, Metal–organic frameworks for solar energy conversion by photoredox catalysis, Coord. Chem. Rev. 373 (2018) 83–115.
[13] A.L. Linsebigler, G. Lu, J.T. Yates Jr., Photocatalysis on TiO2 surfaces: principles, mechanisms, and selected results, Chem. Rev. 95 (1995) 735–758.
[14] B. Li, C. Lai, G. Zeng, L. Qin, H. Yi, D. Huang, C. Zhou, X. Liu, M. Cheng, P. Xu,

C. Zhang, F. Huang, S. Liu, Facile hydrothermal synthesis of Z-scheme Bi2Fe4O9/Bi2WO6 heterojunction photocatalyst with enhanced visible light photocatalytic activity, ACS Appl. Mater. Interfaces 10 (2018) 18824–18836.
[15] C. Lai, M. Zhang, B. Li, D. Huang, G. Zeng, L. Qin, X. Liu, H. Yi, M. Cheng, L. Li, Fabrication of CuS/$BiVO_4$ (0 4 0) binary heterojunction photocatalysts with enhanced photocatalytic activity for Ciprofloxacin degradation and mechanism insight, Chem. Eng. J. 358 (2019) 891–902.
[16] C. Yang, B.C. Ma, L. Zhang, S. Lin, S. Ghasimi, K. Landfester, K.A. Zhang, X. Wang, Molecular engineering of conjugated polybenzothiadiazoles for enhanced hydrogen production by photosynthesis, Angew. Chem. Int. Ed. 55 (2016) 9202–9206.
[17] A. Izgorodin, O. Winther-Jensen, D.R. MacFarlane, On the stability of water oxidation catalysts: challenges and prospects, Aust. J. Chem. 65 (2012) 638.
[18] M. Kitano, M. Matsuoka, M. Ueshima, M. Anpo, Recent developments in titanium oxide-based photocatalysts, Appl. Catal. A 325 (2007) 1–14.
[19] L. Jiao, Y. Wang, H.L. Jiang, Q. Xu, Metal-organic frameworks as platforms for catalytic applications, Adv. Mater. 30 (2018) 1703663.
[20] R. Li, W. Zhang, K. Zhou, Metal–organic-framework-based catalysts for photoreduction of CO2, Adv. Mater. 30 (2018) 1705512.
[21] C. Sun, Q. Dong, J. Yang, Z. Dai, J. Lin, P. Chen, W. Huang, X. Dong, Metal-organic framework derived CoSe 2 nanoparticles anchored on carbon fibers as bifunctional electrocatalysts for efficient overall water splitting, Nano Res. 9 (2016) 2234–2243.
[22] W. Xiong, Z. Zeng, X. Li, G. Zeng, R. Xiao, Z. Yang, Y. Zhou, C. Zhang, M. Cheng, L. Hu, Multi-walled carbon nanotube/amino-functionalized MIL-53 (Fe) composites: remarkable adsorptive removal of antibiotics from aqueous solutions, Chemosphere 210 (2018) 1061–1069.
[23] D. Jiang, M. Chen, H. Wang, G. Zeng, D. Huang, M. Cheng, Y. Liu, W. Xue, Z. Wang, The application of different typological and structural MOFs-based materials for the dyes adsorption, Coord. Chem. Rev. 380 (2019) 471–483.
[24] Y. Fang, J. Wen, G. Zeng, F. Jia, S. Zhang, Z. Peng, H. Zhang, Effect of mineralizing agents on the adsorption performance of metal–organic framework MIL-100 (Fe) towards chromium (VI), Chem. Eng. J. 337 (2018) 532–540.
[25] M. Cheng, C. Lai, Y. Liu, G. Zeng, D. Huang, C. Zhang, L. Qin, L. Hu, C. Zhou, W. Xiong, Metal-organic frameworks for highly efficient heterogeneous Fenton-like catalysis, Coord. Chem. Rev. 368 (2018) 80–92.
[26] M. Campbell, M. Dincă, Metal–organic frameworks as active materials in electronic sensor devices, Sensors 17 (2017) 1108.
[27] W. Xiong, G. Zeng, Z. Yang, Y. Zhou, C. Zhang, M. Cheng, Y. Liu, L. Hu, J. Wan, C. Zhou, Adsorption of tetracycline antibiotics from aqueous solutions on nanocomposite multi-walled carbon nanotube functionalized MIL-53(Fe) as new adsorbent, Sci. Total Environ. 627 (2018) 235–244.
[28] Oliver Kröcher, Sandro Brandenberger, Roderik Althoff, Arno Tissler, The state of the art in selective catalytic reduction of NOx by ammonia using metal-exchanged zeolite catalysts, Catal. Rev. 50 (2008) 492–531.
[29] C. Zhang, W. Wang, A. Duan, G. Zeng, D. Huang, C. Lai, X. Tan, M. Cheng, R. Wang, C. Zhou, Adsorption behavior of engineered carbons and carbon nanomaterials for metal endocrine disruptors: experiments and theoretical calculation, Chemosphere 222 (2019) 184–194.
[30] D. Huang, L. Liu, G. Zeng, P. Xu, C. Huang, L. Deng, R. Wang, J. Wan, The effects of rice straw biochar on indigenous microbial community and enzymes activity in heavy metal-contaminated sediment, Chemosphere 174 (2017) 545–553.
[31] H. Wang, Z. Zeng, P. Xu, L. Li, G. Zeng, R. Xiao, Z. Tang, D. Huang, L. Tang, C. Lai, Recent progress in covalent organic framework thin films: fabrications, applications and perspectives, Chem. Soc. Rev. 48 (2019) 488–516.
[32] Y. Wang, Y. Zhu, Y. Hu, G. Zeng, Y. Zhang, C. Zhang, C. Feng, How to construct DNA hydrogels for environmental applications: advanced water treatment and environmental analysis, Small 14 (2018) 1703305.
[33] J.W. Maina, C. Pozo-Gonzalo, L. Kong, J. Schütz, M. Hill, L.F. Dumée, Metal organic framework based catalysts for CO2 conversion, Mater. Horiz. 4 (2017) 345–361.
[34] W. Wang, X. Xu, W. Zhou, Z. Shao, Recent progress in metal-organic frameworks for applications in electrocatalytic and photocatalytic water splitting, Adv. Sci. 4 (2017) 1600371.
[35] Y. Shi, A.-F. Yang, C.-S. Cao, B. Zhao, Applications of MOFs: recent advances in photocatalytic hydrogen production from water, Coord. Chem. Rev. 390 (2019) 50–75.
[36] A. Kudo, Y. Miseki, Heterogeneous photocatalyst materials for water splitting, Chem. Soc. Rev. 38 (2009) 253–278.
[37] T. Hisatomi, J. Kubota, K. Domen, Recent advances in semiconductors for photocatalytic and photoelectrochemical water splitting, Chem. Soc. Rev. 43 (2014) 7520–7535.
[38] X. Zhang, L. Yu, C. Zhuang, T. Peng, R. Li, X. Li, Highly asymmetric phthalocyanine as a sensitizer of graphitic carbon nitride for extremely efficient photocatalytic H2 production under near-infrared light, ACS Catal. 4 (2013) 162–170.
[39] G. Cui, W. Wang, M. Ma, J. Xie, X. Shi, N. Deng, J. Xin, B. Tang, IR-driven photocatalytic water splitting with WO2–Na x WO3 hybrid conductor material, Nano Lett. 15 (2015) 7199–7203.
[40] X. Chen, C. Li, M. Gratzel, R. Kostecki, S.S. Mao, Nanomaterials for renewable energy production and storage, Chem. Soc. Rev. 41 (2012) 7909–7937.
[41] K. Maeda, K. Domen, New non-oxide photocatalysts designed for overall water splitting under visible light, J. Phys. Chem. C 111 (2007) 7851–7861.
[42] Y. Jinhui, W. Donge, H. Hongxian, L. Can, Roles of cocatalysts in photocatalysis and photoelectrocatalysis, Acc. Chem. Res. 46 (2013) 1900–1909.
[43] H. Liu, C. Xu, D. Li, H.L. Jiang, Photocatalytic hydrogen production coupled with selective benzylamine oxidation over MOF composites, Angew. Chem. Int. Ed. 130 (2018) 5477–5481.
[44] C. Wang, K.E. deKrafft, W. Lin, Pt nanoparticles@photoactive metal-organic frameworks: efficient hydrogen evolution via synergistic photoexcitation and electron injection, J. Am. Chem. Soc. 134 (2012) 7211–7214.
[45] M. Alvaro, E. Carbonell, B. Ferrer, F.X. Llabres i Xamena, H. Garcia, Semiconductor behavior of a metal-organic framework (MOF), Chemistry 13 (2007) 5106–5112.
[46] M.A. Nasalevich, M.V.D. Veen, F. Kapteijn, J. Gascon, Metal–organic frameworks as heterogeneous photocatalysts: advantages and challenges, CrystEngComm 16 (2014) 4919–4926.
[47] J.G. Santaclara, F. Kapteijn, J. Gascon, M.A.V.D. Veen, Understanding metal-organic-frameworks for photocatalytic solar fuel production, CrystEngComm 19 (2017) 4118–4125.
[48] M. Nasalevich, M. Van der Veen, F. Kapteijn, J. Gascon, Metal–organic frameworks as heterogeneous photocatalysts: advantages and challenges, CrystEngComm 16 (2014) 4919–4926.
[49] H. Yu, T. Toyao, M. Saito, K. Mochizuki, M. Iwata, H. Higashimura, M. Anpo, M. Matsuoka, Visible-light-promoted photocatalytic hydrogen production by using an amino-functionalized Ti(IV) metal-organic framework, J. Phys. Chem. C 116 (2012) 20848–20853.
[50] D. Shi, R. Zheng, M.J. Sun, X. Cao, C.X. Sun, C.J. Cui, C.S. Liu, J. Zhao, M. Du, Semiconductive copper (I)–organic frameworks for efficient light-driven hydrogen generation without additional photosensitizers and cocatalysts, Angew. Chem. Int. Ed. 56 (2017) 14637–14641.
[51] S. Pullen, S. Ott, Photochemical hydrogen production with metal-organic frameworks, Top. Catal. 59 (2016) 1712–1721.
[52] X. Wang, T. He, S. Chen, B. Ni, Y. Gong, Z. Wu, L. Song, L. Gu, W. Hu, Zirconium-porphyrin based metal-organic framework hollow nanotubes for immobilization of noble metal single atoms, Angew. Chem. Int. Ed. 57 (2018) 3493–3498.
[53] T. Takashi, S. Masakazu, D. Satoru, M. Katsunori, I. Masatoshi, H. Hideyuki, H. Yu, M. Masaya, Development of a Ru complex-incorporated MOF photocatalyst for hydrogen production under visible-light irradiation, Chem. Commun. 50 (2014) 6779–6781.
[54] M.B. Majewski, A.W. Peters, M.R. Wasielewski, J.T. Hupp, O.K. Farha, Metal–organic frameworks as platform materials for solar fuels catalysis, ACS Energy Lett. 3 (2018) 598–611.
[55] C. Gomes Silva, I. Luz, F.X. Llabres i Xamena, A. Corma, H. Garcia, Water stable Zr-benzenedicarboxylate metal-organic frameworks as photocatalysts for hydrogen generation, Chemistry 16 (2010) 11133–11138.
[56] M. Wen, K. Mori, T. Kamegawa, H. Yamashita, Amine-functionalized MIL-101(Cr) with imbedded platinum nanoparticles as a durable photocatalyst for hydrogen production from water, Chem. Commun. 50 (2014) 11645–11648.
[57] Y. Horiuchi, T. Toyao, K. Miyahara, L. Zakary, D.D. Van, Y. Kamata, T.H. Kim, S.W. Lee, M. Matsuoka, Visible-light-driven photocatalytic water oxidation catalysed by iron-based metal-organic frameworks, Chem. Commun. 52 (2016) 5190–5193.
[58] L. Chi, Q. Xu, X. Liang, J. Wang, X. Su, Iron-based metal-organic frameworks as catalysts for visible light-driven water oxidation, Small 12 (2016) 1351–1358.
[59] X. Wang, X. Zhang, W. Zhou, L. Liu, J. Ye, D. Wang, An ultrathin porphyrin-based metal-organic framework for efficient photocatalytic hydrogen evolution under visible light, Nano Energy 62 (2019) 250–258.
[60] C.C. Hou, T.T. Li, S. Cao, Y. Chen, W.F. Fu, Incorporation of a [Ru(dcbpy)(bpy)2] 2+ photosensitizer and a Pt(dcbpy)Cl2 catalyst into metal-organic frameworks for photocatalytic hydrogen evolution from aqueous solution, J. Mater. Chem. A 3 (2015) 10386–10394.
[61] D. Kim, D.R. Whang, S.Y. Park, Self-healing of molecular catalyst and photosensitizer on metal-organic framework: robust molecular system for photocatalytic H2 evolution from water, J. Am. Chem. Soc. 138 (2016) 8698–8701.
[62] J. Wang, Y. Liu, Y. Li, L. Xia, M. Jiang, P. Wu, Highly efficient visible-light-driven H2 production via an eosin Y-based metal-organic framework, Inorg. Chem. 57 (2018) 7495–7498.
[63] T. Song, P. Zhang, J. Zeng, T. Wang, A. Ali, H. Zeng, Tunable conduction band energy and metal-to-ligand charge transfer for wide-spectrum photocatalytic H2 evolution and stability from isostructural metal-organic frameworks, Int. J. Hydrogen Energy 42 (2017) 26605–26616.
[64] T. Song, L. Zhang, P. Zhang, J. Zeng, T. Wang, A. Ali, H. Zeng, Stable and improved visible-light photocatalytic hydrogen evolution using copper (ii)–organic frameworks: engineering the crystal structures, J. Mater. Chem. A 5 (2017) 6013–6018.
[65] N. Elgrishi, M.B. Chambers, X. Wang, M. Fontecave, Molecular polypyridine-based metal complexes as catalysts for the reduction of CO2, Chem. Soc. Rev. 46 (2017) 761–796.
[66] S. Pullen, H. Fei, A. Orthaber, S.M. Cohen, S. Ott, Enhanced photochemical hydrogen production by a molecular diiron catalyst incorporated into a metal-organic framework, J. Am. Chem. Soc. 135 (2013) 16997–17003.
[67] S. Roy, V. Pascanu, S. Pullen, M.G. González, B. Martínmatute, S. Ott, Catalyst accessibility to chemical reductants in metal-organic frameworks, Chem. Commun. 53 (2017) 3257–3260.
[68] K. Sasan, Q. Lin, C. Mao, P. Feng, Incorporation of iron hydrogenase active sites into a highly stable metal-organic framework for photocatalytic hydrogen generation, Chem. Commun. 50 (2014) 10390–10393.
[69] W.M. Liao, J.H. Zhang, Z. Wang, S.Y. Yin, C.Y. Su, Post-synthetic exchange (PSE) of UiO-67 frameworks by Ru/Rh half-sandwich units for visible-light-driven H2 evolution and CO2 reduction, J. Mater. Chem. A 6 (2018) 11337–11345.
[70] M. Dan-Hardi, C. Serre, T. Frot, L. Rozes, G. Maurin, C. Sanchez, G. Férey, A New photoactive crystalline highly porous titanium(IV) dicarboxylate, J. Am. Chem.

Soc. 131 (2009) 10857–10859.
[71] C.H. Hendon, D. Tiana, M. Fontecave, C. Sanchez, L. D'Arras, C. Sassoye, L. Rozes, C. Mellot-Draznieks, A. Walsh, Engineering the optical response of the titanium-MIL-125 metal-organic framework through ligand functionalization, J. Am. Chem. Soc. 135 (2013) 10942–10945.
[72] Y. Horiuchi, T. Toyao, M. Saito, K. Mochizuki, M. Iwata, H. Higashimura, M. Anpo, M. Matsuoka, Visible-light-promoted photocatalytic hydrogen production by using an amino-functionalized Ti (IV) metal–organic framework, J. Phys. Chem. C 116 (2012) 20848–20853.
[73] T. Toyao, M. Saito, H. Yu, K. Mochizuki, M. Iwata, H. Higashimura, M. Matsuoka, Efficient hydrogen production and photocatalytic reduction of nitrobenzene over a visible-light-responsive metal-organic framework photocatalyst, Catal. Sci. Technol. 3 (2013) 2092–2097.
[74] M. Nasalevich, R. Becker, E.V.R. Fernandez, S. Castellanos, S.L. Veber, M.V. Fedin, F. Kapteijn, J.N.H. Reek, J.I.V.D. Vlugt, J. Gascon, Co@NH2-MIL-125(Ti): cobaloxime-derived metal-organic framework-based composite for light-driven H2 production, Energy Environ. Sci. 8 (2015) 364–375.
[75] A. Iglesias-Juez, S. Castellanos, M. Monte, G. Agostini, D. Osadchii, M.A. Nasalevich, J.G. Santaclara, A.I.O. Suarez, S.L. Veber, M.V. Fedin, Illuminating the nature and behavior of the active center: the key for photocatalytic H2 production in Co@NH2-MIL-125(Ti), J. Mater. Chem. A 6 (2018) 17318–17322.
[76] D. Sun, W. Liu, M. Qiu, Y. Zhang, Z. Li, Introduction of a mediator for enhancing photocatalytic performance via post-synthetic metal exchange in metal-organic frameworks (MOFs), Chem. Commun. 51 (2015) 2056–2059.
[77] A. Fateeva, P.A. Chater, C.P. Ireland, A.A. Tahir, Y.Z. Khimyak, P.V. Wiper, J.R. Darwent, M.J. Rosseinsky, A water-stable porphyrin-based metal-organic framework active for visible-light photocatalysis, Angew. Chem. Int. Ed. 51 (2012) 7440–7444.
[78] A. Aziz, A.R. Ruiz-Salvador, N.C. Hernández, S. Calero, S. Hamad, R. Grau-Crespo, Porphyrin-based metal-organic frameworks for solar fuel synthesis photocatalysis: band gap tuning via iron substitutions, J. Mater. Chem. A 5 (2017) 11894–11904.
[79] R. Grau-Crespo, A. Aziz, A.W. Collins, R. Crespo-Otero, N.C. Hernández, L.M. Rodriguez-Albelo, A.R. Ruiz-Salvador, S. Calero, S. Hamad, Modelling a linker mix-and-match approach for controlling the optical excitation gaps and band alignment of zeolitic imidazolate frameworks, Angew. Chem. 55 (2016) 16012–16016.
[80] J. Qiu, X. Zhang, Y. Feng, X. Zhang, H. Wang, J. Yao, Modified metal-organic frameworks as photocatalysts, Appl. Catal. B 231 (2018) 317–342.
[81] T. Zhang, W. Lin, Metal–organic frameworks for artificial photosynthesis and photocatalysis, Chem. Soc. Rev. 43 (2014) 5982–5993.
[82] P. Wu, M. Jiang, Y. Li, Y. Liu, J. Wang, Highly efficient photocatalytic hydrogen production from pure water via a photoactive metal–organic framework and its PDMS@MOF, J. Mater. Chem. A 5 (2017) 7833–7838.
[83] Y. Yang, Z. Zeng, Z. Chen, D. Huang, G. Zeng, X. Rong, L. Cui, C. Zhou, G. Hai, W. Xue, Construction of iodine vacancy-rich BiOI/Ag@AgI Z-scheme heterojunction photocatalysts for visible-light-driven tetracycline degradation: transformation pathways and mechanism insight, Chem. Eng. J. 349 (2018) 808–821.
[84] C. Zhou, C. Lai, D. Huang, G. Zeng, C. Zhang, M. Cheng, L. Hu, J. Wan, W. Xiong, M. Wen, X. Wen, L. Qin, Highly porous carbon nitride by supramolecular preassembly of monomers for photocatalytic removal of sulfamethazine under visible light driven, Appl. Catal. B 220 (2018) 202–210.
[85] W. Wang, Z. Zeng, G. Zeng, C. Zhang, R. Xiao, C. Zhou, W. Xiong, Y. Yang, L. Lei, Y. Liu, Sulfur doped carbon quantum dots loaded hollow tubular g-C3N4 as novel photocatalyst for destruction of Escherichia coli and tetracycline degradation under visible light, Chem. Eng. J. 378 (2019) 122132.
[86] D. He, C. Zhang, G. Zeng, Y. Yang, D. Huang, L. Wang, H. Wang, A multifunctional platform by controlling of carbon nitride in the core-shell structure: from design to construction, and catalysis applications, Appl. Catal. B 258 (2019) 117957.
[87] C. Zhou, P. Xu, C. Lai, C. Zhang, G. Zeng, D. Huang, M. Cheng, L. Hu, W. Xiong, X. Wen, Rational design of graphic carbon nitride copolymers by molecular doping for visible-light-driven degradation of aqueous sulfamethazine and hydrogen evolution, Chem. Eng. J. 359 (2019) 186–196.
[88] Y. Yang, C. Zhang, D. Huang, G. Zeng, J. Huang, C. Lai, C. Zhou, W. Wang, H. Guo, W. Xue, Boron nitride quantum dots decorated ultrathin porous g-C3N4: intensified exciton dissociation and charge transfer for promoting visible-light-driven molecular oxygen activation, Appl. Catal. B 245 (2019) 87–99.
[89] W. Wang, P. Xu, M. Chen, G. Zeng, C. Zhang, C. Zhou, Y. Yang, D. Huang, C. Lai, M. Cheng, Alkali metal-assisted synthesis of graphite carbon nitride with tunable band-gap for enhanced visible-light-driven photocatalytic performance, ACS Sustain. Chem. Eng. 6 (2018) 15503–15516.
[90] R. Wang, L. Gu, J. Zhou, X. Liu, F. Teng, C. Li, Y. Shen, Y. Yuan, Quasi-polymeric metal-organic framework UiO-66/g-C3N4 heterojunctions for enhanced photocatalytic hydrogen evolution under visible light irradiation, Adv. Mater. Interfaces 2 (2015) 1500037.
[91] A. Cao, L. Zhang, Y. Wang, H. Zhao, H. Deng, X. Liu, Z. Lin, X. Su, F. Yue, 2D–2D heterostructured UNiMOF/g-C3N4 for enhanced photocatalytic H2 production under visible-light irradiation, ACS Sustain. Chem. Eng. 7 (2018) 2492–2499.
[92] G. Zhou, M.F. Wu, Q.J. Xing, F. Li, H. Liu, X.B. Luo, J.P. Zou, J.M. Luo, A.Q. Zhang, Synthesis and characterizations of metal-free semiconductor/MOFs with good stability and high photocatalytic activity for H2 evolution: a novel Z-Scheme heterostructured photocatalyst formed by covalent bonds, Appl. Catal. B 220 (2018) 607–614.
[93] L. Qin, D. Huang, P. Xu, G. Zeng, C. Lai, Y. Fu, H. Yi, B. Li, C. Zhang, M. Cheng, In-situ deposition of gold nanoparticles onto polydopamine-decorated g-C3N4 for highly efficient reduction of nitroaromatics in environmental water purification, J. Colloid Interface Sci. 534 (2019) 357–369.
[94] J. Xu, J. Gao, C. Wang, Y. Yang, L. Wang, NH2-MIL-125(Ti)/graphitic carbon nitride heterostructure decorated with NiPd co-catalysts for efficient photocatalytic hydrogen production, Appl. Catal. B 219 (2017) 101–108.
[95] Y. Wang, F. Wang, J. He, Controlled fabrication and photocatalytic properties of a three-dimensional ZnO nanowire/reduced graphene oxide/CdS heterostructure on carbon cloth, Nanoscale 5 (2013) 11291–11297.
[96] J. He, Z. Yan, J. Wang, J. Xie, L. Jiang, Y. Shi, F. Yuan, F. Yu, Y. Sun, Significantly enhanced photocatalytic hydrogen evolution under visible light over CdS embedded on metal-organic frameworks, Chem. Commun. 49 (2013) 6761–6763.
[97] J.-J. Zhou, R. Wang, X.-L. Liu, F.-M. Peng, C.-H. Li, F. Teng, Y.-P. Yuan, In situ growth of CdS nanoparticles on UiO-66 metal-organic framework octahedrons for enhanced photocatalytic hydrogen production under visible light irradiation, Appl. Surf. Sci. 346 (2015) 278–283.
[98] Y. Wang, Y. Zhang, Z. Jiang, G. Jiang, Z. Zhao, Q. Wu, Y. Liu, Q. Xu, A. Duan, C. Xu, Controlled fabrication and enhanced visible-light photocatalytic hydrogen production of Au@CdS/MIL-101 heterostructure, Appl. Catal. B 185 (2016) 307–314.
[99] X.-B. Meng, J.-L. Sheng, H.-L. Tang, X.-J. Sun, H. Dong, F.-M. Zhang, Metal-organic framework as nanoreactors to co-incorporate carbon nanodots and CdS quantum dots into the pores for improved H2 evolution without noble-metal cocatalyst, Appl. Catal. B 244 (2019) 340–346.
[100] Y. Su, Z. Zhang, H. Liu, Y. Wang, Cd 0.2 Zn 0.8 S@UiO-66-NH 2 nanocomposites as efficient and stable visible-light-driven photocatalyst for H 2 evolution and CO 2 reduction, Appl. Catal. B 200 (2017) 448–457.
[101] Q. Liang, J. Jin, C. Liu, S. Xu, C. Yao, Z. Li, Fabrication of the ternary heterojunction Cd0.5Zn0.5S@UIO-66@g-C3N4 for enhanced visible-light photocatalytic hydrogen evolution and degradation of organic pollutants, Inorg. Chem. Front. 5 (2018) 335–343.
[102] T.F. Jaramillo, K.P. JøRgensen, B. Jacob, J.H. Nielsen, H. Sebastian, C. Ib, Identification of active edge sites for electrochemical H2 evolution from MoS2 nanocatalysts, Science 317 (2007) 100–102.
[103] L. Shen, M. Luo, Y. Liu, R. Liang, F. Jing, L. Wu, Noble-metal-free MoS2 co-catalyst decorated UiO-66/CdS hybrids for efficient photocatalytic H2 production, Appl. Catal. B 166-167 (2015) 445–453.
[104] P. Karthik, E. Balaraman, B. Neppolian, Efficient solar light-driven H2 production: post-synthetic encapsulation of a Cu2O co-catalyst in a metal–organic framework (MOF) for boosting the effective charge carrier separation, Catal. Sci. Technol. 8 (2018) 3286–3294.
[105] M. Zhang, Q. Shang, Y. Wan, Q. Cheng, G. Liao, Z. Pan, Self-template synthesis of double-shell TiO2@ ZIF-8 hollow nanospheres via sonocrystallization with enhanced photocatalytic activities in hydrogen generation, Appl. Catal. B 241 (2019) 149–158.
[106] H. Kai, G. Chen, G. Zeng, A. Chen, Z. Huang, J. Shi, T. Huang, P. Min, H. Liang, Three-dimensional graphene supported catalysts for organic dyes degradation, Appl. Catal. B 228 (2018) 19–28.
[107] K. He, Z. Zeng, A. Chen, G. Zeng, R. Xiao, P. Xu, Z. Huang, J. Shi, L. Hu, G. Chen, Advancement of Ag-graphene based nanocomposites: an overview of synthesis and its applications, Small 14 (2018) 1800871.
[108] J.S. Lee, K.H. You, C.B. Park, Highly photoactive, low bandgap TiO2 nanoparticles wrapped by graphene, Adv. Mater. 24 (2012) 1084–1088.
[109] Y. Wang, Y. Yu, R. Li, H. Liu, W. Zhang, L. Ling, W. Duan, B. Liu, Hydrogen production with ultrahigh efficiency under visible light by graphene well-wrapped UiO-66-NH2 octahedrons, J. Mater. Chem. A 5 (2017) 20136–20140.
[110] D. Liu, Z. Jin, Y. Zhang, G. Wang, B. Ma, Light harvesting and charge management by Ni4S3 modified metal-organic frameworks and rGO in the process of photocatalysis, J. Colloid Interface Sci. 529 (2018) 44–52.
[111] X. Shi, J. Zhang, G. Cui, N. Deng, W. Wang, Q. Wang, B. Tang, Photocatalytic H2 evolution improvement for H free-radical stabilization by electrostatic interaction of a Cu-BTC MOF with ZnO/GO, Nano Res. 11 (2017) 979–987.
[112] L. Rui, S. Lijuan, R. Zhuyun, W. Weiming, T. Yanxi, F. Hongru, Z. Jian, W. Ling, Enhanced photocatalytic hydrogen production activity via dual modification of MOF and reduced graphene oxide on CdS, Chem. Commun. 50 (2014) 8533–8535.
[113] X. Hao, Z. Jin, H. Yang, G. Lu, Y. Bi, Peculiar synergetic effect of MoS 2 quantum dots and graphene on metal-organic frameworks for photocatalytic hydrogen evolution, Appl. Catal. B 210 (2017) 45–56.
[114] Z. Huang, K. He, Z. Song, G. Zeng, A. Chen, L. Yuan, H. Li, L. Hu, Z. Guo, G. Chen, Antioxidative response of Phanerochaete chrysosporium against silver nanoparticle-induced toxicity and its potential mechanism, Chemosphere 211 (2018) 573–583.
[115] L. Qin, G. Zeng, C. Lai, D. Huang, P. Xu, C. Zhang, M. Cheng, X. Liu, S. Liu, B. Li, "Gold rush" in modern science: fabrication strategies and typical advanced applications of gold nanoparticles in sensing, Coord. Chem. Rev. 359 (2018) 1–31.
[116] C. Zhou, C. Lai, C. Zhang, G. Zeng, D. Huang, M. Cheng, L. Hu, W. Xiong, M. Chen, J. Wang, Semiconductor/boron nitride composites: synthesis, properties, and photocatalysis applications, Appl. Catal. B 238 (2018) 6–18.
[117] C. Zhang, C. Lai, G. Zeng, D. Huang, C. Yang, Y. Wang, Y. Zhou, M. Cheng, Efficacy of carbonaceous nanocomposites for sorbing ionizable antibiotic sulfamethazine from aqueous solution, Water Res. 95 (2016) 103–112.
[118] L. Zhang, J. Zhang, G. Zeng, H. Dong, Y. Chen, C. Huang, Y. Zhu, R. Xu, Y. Cheng, K. Hou, Multivariate relationships between microbial communities and environmental variables during co-composting of sewage sludge and agricultural waste in the presence of PVP-AgNPs, Bioresour. Technol. 261 (2018) 10–18.
[119] D. Sun, Z. Li, Double-solvent method to Pd nanoclusters encapsulated inside the cavity of NH2–Uio-66(Zr) for efficient visible-light-promoted suzuki coupling reaction, J. Phys. Chem. C 120 (2016) 19744–19750.

[120] L. Qin, G. Zeng, C. Lai, D. Huang, C. Zhang, P. Xu, T. Hu, X. Liu, M. Cheng, Y. Liu, A visual application of gold nanoparticles: simple, reliable and sensitive detection of kanamycin based on hydrogen-bonding recognition, Sens. Actuators B 243 (2017) 946–954.

[121] D. Huang, Z. Hu, Z. Peng, G. Zeng, G. Chen, C. Zhang, M. Cheng, J. Wan, X. Wang, X. Qin, Cadmium immobilization in river sediment using stabilized nanoscale zero-valent iron with enhanced transport by polysaccharide coating, J. Environ. Manage. 210 (2018) 191–200.

[122] W. Wang, C.F. Anderson, Z. Wang, W. Wu, H. Cui, C.J. Liu, Peptide-templated noble metal catalysts: syntheses and applications, Chem. Sci. 8 (2017) 3310–3324.

[123] J.D. Xiao, Q. Shang, Y. Xiong, Q. Zhang, Y. Luo, S.H. Yu, H.L. Jiang, Boosting photocatalytic hydrogen production of a metal-organic framework decorated with platinum nanoparticles: the platinum location matters, Angew. Chem. 55 (2016) 9389–9393.

[124] Y. Xiao, Y. Qi, X. Wang, X. Wang, F. Zhang, C. Li, Visible-light-responsive 2D cadmium-organic framework single crystals with dual functions of water reduction and oxidation, Adv. Mater. 30 (2018) 1803401.

[125] L. Shen, M. Luo, L. Huang, P. Feng, L. Wu, A clean and general strategy to decorate a titanium metal-organic framework with noble-metal nanoparticles for versatile photocatalytic applications, Inorg. Chem. 54 (2015) 1191–1193.

[126] D. Li, S.H. Yu, H.L. Jiang, From UV to near-infrared light-responsive metal-organic framework composites: plasmon and upconversion enhanced photocatalysis, Adv. Mater. 30 (2018) 1707377.

[127] Z. Wang, Z. Jin, H. Yuan, G. Wang, B. Ma, Orderly-designed Ni2P nanoparticles on g-C3N4 and UiO-66 for efficient solar water splitting, J. Colloid Interface Sci. 532 (2018) 287–299.

[128] S. Kampouri, T.N. Nguyen, C.P. Ireland, B. Valizadeh, F.M. Ebrahim, G. Capano, D. Ongari, A. Mace, N. Guijarro, K. Sivula, A. Sienkiewicz, L. Forró, B. Smit, K.C. Stylianou, Photocatalytic hydrogen generation from a visible-light responsive metal–organic framework system: the impact of nickel phosphide nanoparticles, J. Mater. Chem. A 6 (2018) 2476–2481.

[129] C.C. Shen, Y.N. Liu, X. Wang, X.X. Fang, Z.W. Zhao, N. Jiang, L.B. Ma, X. Zhou, T.Y. Cheang, A.W. Xu, Boosting visible-light photocatalytic H2 evolution via UiO-66-NH2 octahedrons decorated with ultrasmall NiO nanoparticles, Dalton Trans. 47 (2018) 11705–11712.

[130] H. Tributsch, Dye sensitization solar cells: a critical assessment of the learning curve, Coord. Chem. Rev. 248 (2004) 1511–1530.

[131] X.-L. Liu, R. Wang, M.-Y. Zhang, Y.-P. Yuan, C. Xue, Dye-sensitized MIL-101 metal organic frameworks loaded with Ni/NiOx nanoparticles for efficient visible-light-driven hydrogen generation, APL Mater. 3 (2015) 104403.

[132] Y.-P. Yuan, L.-S. Yin, S.-W. Cao, G.-S. Xu, C.-H. Li, C. Xue, Improving photocatalytic hydrogen production of metal–organic framework UiO-66 octahedrons by dye-sensitization, Appl. Catal. B 168-169 (2015) 572–576.

[133] Y.-F. Chen, L.-L. Tan, J.-M. Liu, S. Qin, Z.-Q. Xie, J.-F. Huang, Y.-W. Xu, L.-M. Xiao, C.-Y. Su, Calix[4]arene based dye-sensitized Pt@UiO-66-NH 2 metal-organic framework for efficient visible-light photocatalytic hydrogen production, Appl. Catal. B 206 (2017) 426–433.

[134] H. Li, S. Yao, H.-L. Wu, J.-Y. Qu, Z.-M. Zhang, T.-B. Lu, W. Lin, E.-B. Wang, Charge-regulated sequential adsorption of anionic catalysts and cationic photosensitizers into metal-organic frameworks enhances photocatalytic proton reduction, Appl. Catal. B 224 (2018) 46–52.

[135] Y. Liu, Z. Liu, D. Huang, M. Cheng, G. Zeng, C. Lai, C. Zhang, C. Zhou, W. Wang, D. Jiang, Metal or metal-containing nanoparticle@ MOF nanocomposites as a promising type of photocatalyst, Coordination Chem. Rev. 388 (2019) 63–78.

[136] D.Y. Du, J.S. Qin, S.L. Li, Z.M. Su, Y.Q. Lan, Recent advances in porous polyoxometalate-based metal-organic framework materials, Chem. Soc. Rev. 43 (2014) 4615–4632.

[137] W. Guo, H. Lv, Z. Chen, K.P. Sullivan, S.M. Lauinger, Y. Chi, J.M. Sumliner, T. Lian, C.L. Hill, Self-assembly of polyoxometalates, Pt nanoparticles and metal–organic frameworks into a hybrid material for synergistic hydrogen evolution, J. Mater. Chem. A 4 (2016) 5952–5957.

[138] J. Tian, Z.Y. Xu, D.W. Zhang, H. Wang, S.H. Xie, D.W. Xu, Y.H. Ren, H. Wang, Y. Liu, Z.T. Li, Supramolecular metal-organic frameworks that display high homogeneous and heterogeneous photocatalytic activity for H2 production, Nat. Commun. 7 (2016) 11580.

[139] J. Han, D. Wang, Y. Du, S. Xi, Z. Chen, S. Yin, T. Zhou, R. Xu, Polyoxometalate immobilized in MIL-101(Cr) as an efficient catalyst for water oxidation, Appl. Catal. A 521 (2016) 83–89.

[140] W.A. Shah, A. Waseem, M.A. Nadeem, P. Kögerler, Leaching-free encapsulation of cobalt-polyoxotungstates in MIL-100 (Fe) for highly reproducible photocatalytic water oxidation, Appl. Catal. A 567 (2018) 132–138.

[141] G. Paille, M. Gomez-Mingot, C. Roch-Marchal, B. Lassalle-Kaiser, P. Mialane, M. Fontecave, C. Mellot-Draznieks, A. Dolbecq, A fully noble metal-free photosystem based on cobalt-polyoxometalates immobilized in a porphyrinic metal-organic framework for water oxidation, J. Am. Chem. Soc. 140 (2018) 3613–3618.

[142] X.J. Kong, Z. Lin, Z.M. Zhang, T. Zhang, W. Lin, Hierarchical integration of photosensitizing metal-organic frameworks and nickel-containing polyoxometalates for efficient visible-light-driven hydrogen evolution, Angew. Chem. 128 (2016) 6521–6526.

[143] Z. Jiang, J. Liu, M. Gao, X. Fan, L. Zhang, J. Zhang, Assembling polyoxo-titanium clusters and CdS nanoparticles to a porous matrix for efficient and tunable H2-evolution activities with visible light, Adv. Mater. 29 (2017) 1603369.

[144] M. Cheng, Y. Liu, D. Huang, C. Lai, G. Zeng, J. Huang, Z. Liu, C. Zhang, C. Zhou, L. Qin, Prussian blue analogue derived magnetic Cu-Fe oxide as a recyclable photo-Fenton catalyst for the efficient removal of sulfamethazine at near neutral pH values, Chem. Eng. J. 362 (2019) 865–876.

[145] W. Zhan, L. Sun, X. Han, Recent progress on engineering highly efficient porous semiconductor photocatalysts derived from metal-organic frameworks, Nano-Micro Lett. 11 (2019) 1.

[146] J. Chen, J. Chen, Y. Li, Hollow ZnCdS dodecahedral cages for highly efficient visible-light-driven hydrogen generation, J. Mater. Chem. A 5 (2017) 24116–24125.

[147] L. He, L. Li, T. Wang, H. Gao, G. Li, X. Wu, Z. Su, C. Wang, Fabrication of Au/ZnO nanoparticles derived from ZIF-8 with visible light photocatalytic hydrogen production and degradation dye activities, Dalton Trans. 43 (2014) 16981–16985.

[148] Y. Zhang, J. Huang, Y. Ding, Porous Co3O4/CuO hollow polyhedral nanocages derived from metal-organic frameworks with heterojunctions as efficient photocatalytic water oxidation catalysts, Appl. Catal. B 198 (2016) 447–456.

[149] M. Lan, R.-M. Guo, Y. Dou, J. Zhou, A. Zhou, J.-R. Li, Fabrication of porous Pt-doping heterojunctions by using bimetallic MOF template for photocatalytic hydrogen generation, Nano Energy 33 (2017) 238–246.

[150] Y. Su, S. Li, D. He, D. Yu, F. Liu, N. Shao, Z. Zhang, MOF-derived porous ZnO nanocages/rGO/carbon sponge-based photocatalytic microreactor for efficient degradation of water pollutants and hydrogen evolution, ACS Sustain. Chem. Eng. 6 (2018) 11989–11998.

[151] B. Yan, L. Zhang, Z. Tang, M. Al-Mamun, H. Zhao, X. Su, Palladium-decorated hierarchical titania constructed from the metal-organic frameworks NH2-MIL-125(Ti) as a robust photocatalyst for hydrogen evolution, Appl. Catal. B 218 (2017) 743–750.

[152] P. Xu, G.M. Zeng, D.L. Huang, C.L. Feng, S. Hu, M.H. Zhao, C. Lai, Z. Wei, C. Huang, G.X. Xie, Use of iron oxide nanomaterials in wastewater treatment: a review, Sci. Total Environ. 424 (2012) 1–10.

[153] J. Yao, J. Chen, K. Shen, Y. Li, Phase-controllable synthesis of MOF-templated maghemite–carbonaceous composites for efficient photocatalytic hydrogen production, J. Mater. Chem. A 6 (2018) 3571–3582.

[154] H. Yi, D. Huang, G. Zeng, C. Lai, L. Qin, M. Cheng, S. Ye, B. Song, X. Ren, X. Guo, Selective prepared carbon nanomaterials for advanced photocatalytic application in environmental pollutant treatment and hydrogen production, Appl. Catal. B 239 (2018) 408–424.

[155] J.L. Gong, B. Wang, G.M. Zeng, C.P. Yang, C.G. Niu, Q.Y. Niu, W.J. Zhou, Y. Liang, Removal of cationic dyes from aqueous solution using magnetic multi-wall carbon nanotube nanocomposite as adsorbent, J. Hazard. Mater. 164 (2009) 1517–1522.

[156] X. Zhao, H. Yang, P. Jing, W. Shi, G. Yang, P. Cheng, A metal-organic framework approach toward highly nitrogen-doped graphitic carbon as a metal-free photocatalyst for hydrogen evolution, Small 13 (2017) 1603279.

[157] F. He, G. Chen, Y. Zhou, Y. Yu, L. Li, S. Hao, B. Liu, ZIF-8 derived carbon (C-ZIF) as a bifunctional electron acceptor and HER cocatalyst for g-C3N4: construction of a metal-free, all carbon-based photocatalytic system for efficient hydrogen evolution, J. Mater. Chem. A 4 (2016) 3822–3827.

[158] M. Zhang, Y.-L. Huang, J.-W. Wang, T.-B. Lu, A facile method for the synthesis of a porous cobalt oxide–carbon hybrid as a highly efficient water oxidation catalyst, J. Mater. Chem. A 4 (2016) 1819–1827.

[159] J.D. Xiao, H.L. Jiang, Thermally stable metal-organic framework-templated synthesis of hierarchically porous metal sulfides: enhanced photocatalytic hydrogen production, Small 13 (2017) 1700632.

[160] X. Zhao, J. Feng, J. Liu, W. Shi, G. Yang, G.C. Wang, P. Cheng, An efficient, visible-light-driven, hydrogen evolution catalyst NiS/Znx Cd1-x S nanocrystal derived from a metal-organic framework, Angew. Chem. 57 (2018) 9790–9794.

[161] J. Xu, Y. Qi, C. Wang, L. Wang, NH2-MIL-101(Fe)/Ni(OH)2-derived C, N-codoped Fe2P/Ni2P cocatalyst modified g-C3N4 for enhanced photocatalytic hydrogen evolution from water splitting, Appl. Catal. B 241 (2019) 178–186.

[162] D.P. Kumar, J. Choi, S. Hong, D.A. Reddy, S. Lee, T.K. Kim, Rational synthesis of metal-organic framework-derived noble metal-free nickel phosphide nanoparticles as a highly efficient cocatalyst for photocatalytic hydrogen evolution, ACS Sustain. Chem. Eng. 4 (2016) 7158–7166.

[163] Y. Chao, J. Zheng, J. Chen, Z. Wang, S. Jia, H. Zhang, Z. Zhu, Highly efficient visible light-driven hydrogen production of precious metal-free hybrid photocatalyst: CdS@ NiMoS core–shell nanorods, Catal. Sci. Technol. 7 (2017) 2798–2804.

[164] U. Gupta, B. Naidu, U. Maitra, A. Singh, S.N. Shirodkar, U.V. Waghmare, C. Rao, Characterization of few-layer 1T-MoSe2 and its superior performance in the visible-light induced hydrogen evolution reaction, APL Mater. 2 (2014) 37–38.

[165] S. Cao, Y. Chen, C.-J. Wang, X.-J. Lv, W.-F. Fu, Spectacular photocatalytic hydrogen evolution using metal-phosphide/CdS hybrid catalysts under sunlight irradiation, Chem. Commun. 51 (2015) 8708–8711.

[166] Z. Sun, H. Zheng, J. Li, P. Du, Extraordinarily efficient photocatalytic hydrogen evolution in water using semiconductor nanorods integrated with crystalline Ni 2 P cocatalysts, Energy Environ. Sci. 8 (2015) 2668–2676.

[167] W. Che, W. Cheng, T. Yao, F. Tang, W. Liu, H. Su, Y. Huang, Q. Liu, J. Liu, F. Hu, Fast photoelectron transfer in (Cring)–C3N4 plane heterostructural nanosheets for overall water splitting, J. Am. Chem. Soc. 139 (2017) 3021–3026.

[168] J.-F. Huang, J.-M. Liu, L.-M. Xiao, Y.-H. Zhong, L. Liu, S. Qin, J. Guo, C.-Y. Su, Facile synthesis of porous hybrid materials based on Calix-3 dye and TiO 2 for high photocatalytic water splitting performance with excellent stability, J. Mater. Chem. A 7 (2019) 2993–2999.

[169] J.Y. Zhang, H. Wang, Y. Tian, Y. Yan, Q. Xue, T. He, H. Liu, C. Wang, Y. Chen, B.Y. Xia, Anodic hydrazine oxidation assists energy-efficient hydrogen evolution over a bifunctional cobalt perselenide nanosheet electrode, Angew. Chem. Int. Ed. 57 (2018) 7649–7653.

[170] J.-Y. Zhang, T. He, M. Wang, R. Qi, Y. Yan, Z. Dong, H. Liu, H. Wang, B.Y. Xia, Energy-saving hydrogen production coupling urea oxidation over a bifunctional nickel-molybdenum nanotube array, Nano Energy 60 (2019) 894–902.

[171] T. He, J.M.V. Nsanzimana, R. Qi, J.-Y. Zhang, M. Miao, Y. Yan, K. Qi, H. Liu, B.Y. Xia, Synthesis of amorphous boride nanosheets by the chemical reduction of Prussian blue analogs for efficient water electrolysis, J. Mater. Chem. A 6 (2018) 23289–23294.
[172] F. Yang, A. Chen, P.L. Deng, Y. Zhou, Z. Shahid, H. Liu, B.Y. Xia, Highly efficient electroconversion of carbon dioxide into hydrocarbons by cathodized copper–organic frameworks, Chem. Sci. 10 (2019) 7975–7981.
[173] W. Zhan, Y. Yuan, L. Sun, Y. Yuan, X. Han, Y. Zhao, Hierarchical NiO@ N-doped carbon microspheres with ultrathin nanosheet subunits as excellent photocatalysts for hydrogen evolution, Small 15 (2019) 1901024.